Article

Cell Chemical Biology

N-Thio-β-lactams targeting L,D-transpeptidase-2, with activity against drug-resistant strains of *Mycobacterium tuberculosis*

Graphical abstract

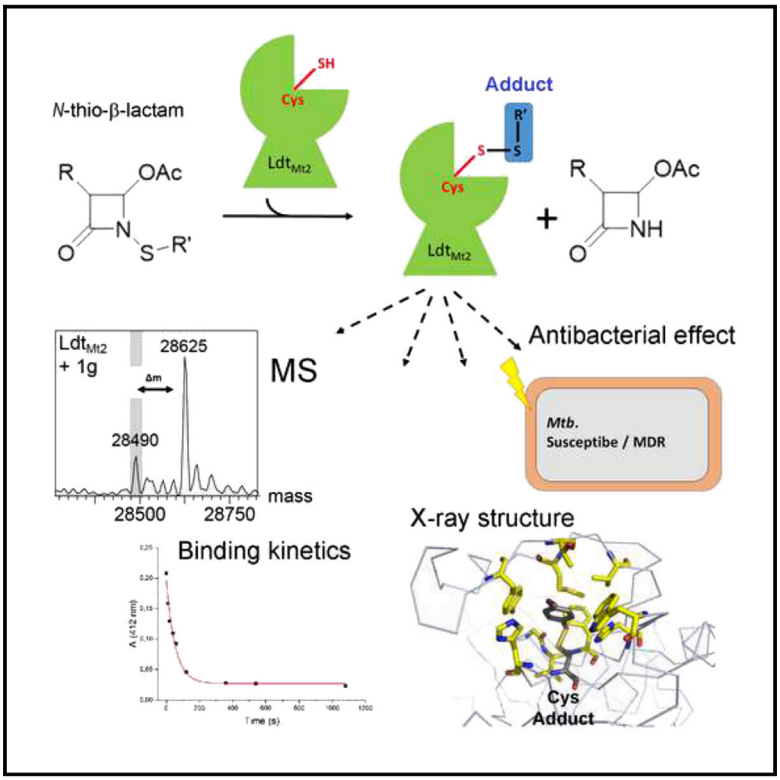

Highlights

- Novel *N*-thio-β-lactams were designed and characterized on L,D-transpeptidase-2
- Five compounds present kinetic binding constants equal or superior to carbapenems
- Mass spectrometry and 5 X-ray structures revealed an unusual mode of adduct formation
- Growth inhibition in the μg/mL range *in vitro* against *Mtb*, including MDR isolates

Authors

Giulia Martelli, Tomas Bohn Pessatti, Eva Maria Steiner, ..., Paola Dal Monte, Daria Giacomini, Robert Schnell

Correspondence

paola.dalmonte@unibo.it (P.D.M.), daria.giacomini@unibo.it (D.G.), robert.schnell@ki.se (R.S.)

In brief

Martelli et al. describe the design, synthesis, and characterization of novel antibiotic candidates targeting *M. tuberculosis*. These compounds inhibit a cell wall remodeling protein using an unconventional mechanism of action acting as effectively as carbapenem-type antibiotics. Furthermore, they kill *M. tuberculosis* including drug-resistant variants *in vitro*.

Martelli et al., 2021, Cell Chemical Biology *28*, 1321–1332
September 16, 2021
https://doi.org/10.1016/j.chembiol.2021.03.008

CellPress

Cell Chemical Biology

CellPress
OPEN ACCESS

Article

N-Thio-β-lactams targeting L,D-transpeptidase-2, with activity against drug-resistant strains of *Mycobacterium tuberculosis*

Giulia Martelli,[1,5] Tomas Bohn Pessatti,[2,5] Eva Maria Steiner,[2] Martina Cirillo,[1] Carolina Caso,[2] Francesco Bisognin,[3] Michael Landreh,[4] Paola Dal Monte,[3,*] Daria Giacomini,[1,*] and Robert Schnell[2,6,*]

[1]Department of Chemistry "G. Ciamician", University of Bologna, Via Selmi 2, 40126 Bologna, Italy
[2]Department of Medical Biochemistry and Biophysics, Karolinska Institutet, 17 165 Stockholm, Sweden
[3]IRCCS Azienda Ospedaliero-Universitaria di Bologna, Microbiology Unit, Via Massarenti, 9, 40138 Bologna, Italy
[4]Department of Microbiology, Tumor and Cell Biology, Karolinska Institutet, 17 165 Stockholm, Sweden
[5]These authors contributed equally
[6]Lead contact
*Correspondence: paola.dalmonte@unibo.it (P.D.M.), daria.giacomini@unibo.it (D.G.), robert.schnell@ki.se (R.S.)
https://doi.org/10.1016/j.chembiol.2021.03.008

SUMMARY

Effective treatment of tuberculosis is frequently hindered by the emerging antimicrobial resistance of *Mycobacterium tuberculosis*. The present study evaluates monocyclic β-lactam compounds targeting the mycobacterial cell wall remodeling. Novel *N*-thio-β-lactams were designed, synthesized, and characterized on the L,D-transpeptidase-2, a validated target in *M. tuberculosis*. The candidates were evaluated in biochemical assays identifying five compounds presenting target-specific kinetic constants equal or superior to meropenem, a carbapenem currently considered for tuberculosis therapy. Mass spectrometry in line with the crystal structures of five target-ligand complexes revealed that the *N*-thio-β-lactams act via an unconventional mode of adduct formation, transferring the thio-residues from the lactam ring to the active-site cysteine of Ldt_{Mt2}. The resulting stable adducts lead to a long-term inactivation of the target protein. Finally, the candidates were evaluated *in vitro* against a drug-susceptible and multidrug-resistant clinical isolates of *M. tuberculosis*, confirming the antimycobacterial effect of these novel compounds.

INTRODUCTION

β-Lactams are a well-known class of antibacterial agents characterized by the crucial structural scaffold of the four-membered azetidin-2-one ring. Along with bicyclic β-lactams such as penicillins, cephalosporins, and the later developed carbapenems, the discovery of some monocyclic molecules in the early 1980s, known as nocardicines and aztreonam, served the first evidence that the bicyclic structure was not essential to gain antibacterial activity (Figure 1A) (Cimarusti and Sykes, 1984). β-Lactam antibiotics are still the main class of agents used today to treat bacterial infections, and a plethora of monocyclic β-lactams available today exhibit potent antimicrobial effects and diverse biological activities (Galletti and Giacomini, 2011; Decuyper et al., 2018). The emergence of antibiotic resistance, however, presents one of the greatest challenges today in the management of infectious diseases. A number of human pathogens including *Mycobacterium tuberculosis*, the causative agent of tuberculosis (TB), presents a serious problem with the increased occurrence of antimicrobial resistance and with the emergence of multidrug-resistant (MDR) infections observed in the clinic. Consequently, the World Health Organization considers the development of novel and effective antibiotics against MDR *M. tuberculosis* a high-priority issue (Tacconelli et al., 2018; Tacconelli and Pezzani, 2019; European Center for Disease Prevention and Control, 2018).

The mycobacterial cell envelope is more complex than the cell wall of Gram-positive or Gram-negative bacteria and is an established target for antibiotics including specific antitubercular agents which act by interfering with cell wall stability and maintenance. This multilayered structure is in part responsible for the increased stress tolerance and for the relatively low permeability to antibiotics, a characteristic of *M. tuberculosis* (Dulberger et al., 2020; Jankute et al., 2015). In addition to this protective barrier the expression of efflux pumps, β-lactamases (BLA), and modified peptidoglycan structure contribute to the increased antibiotic tolerance of this pathogen (Wivagg et al., 2014).

In the mycobacterial cell wall the peptidoglycan layer is situated at the innermost position, forms the foundation of the complex multilayered structure, and is responsible for the mechanical and osmotic stability (Dulberger et al., 2020, Wivagg et al., 2014; Vollmer et al., 2008). Peptidoglycan (PG) is a complex polymer (Figure 1B) built by carbohydrate (glycan) chains of alternating *N*-acetylglycosamine and *N*-acetylmuramic acid

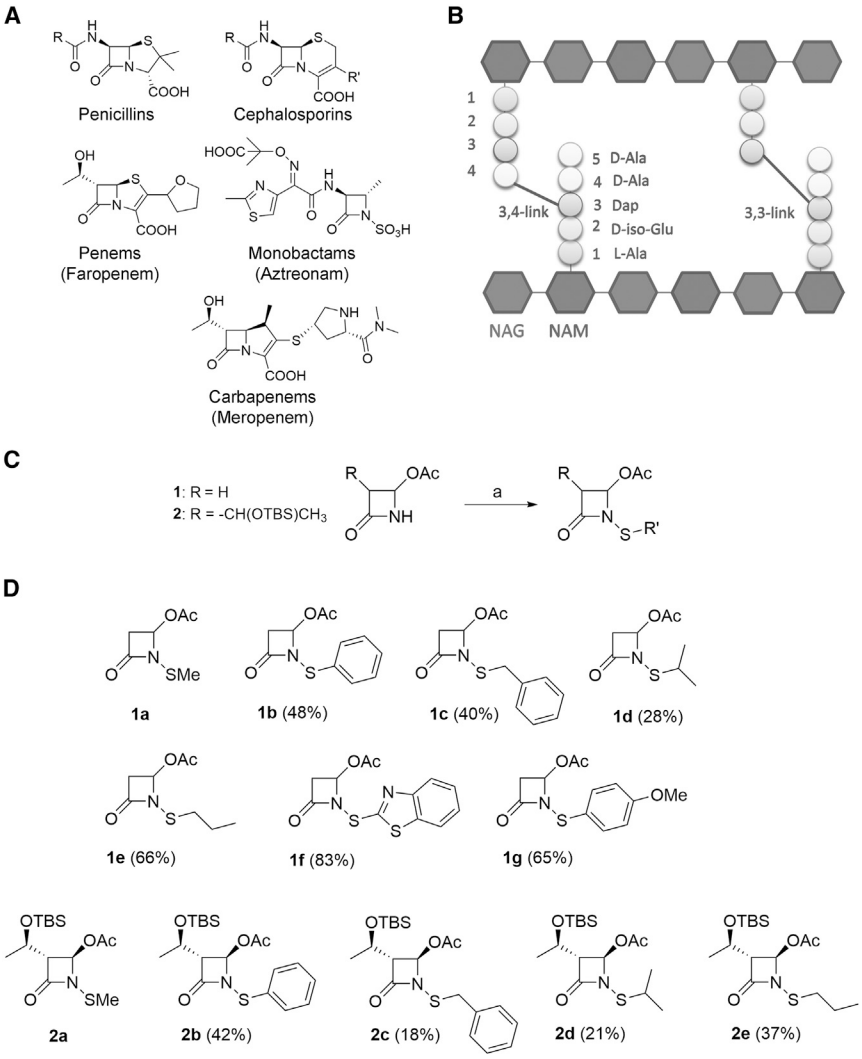

Figure 1. ß-Lactam antibiotics and *N*-thio-ß-lactams

(A) β-Lactam antibiotics representing the main classes.

(B) Schematic structure of the cell wall peptidoglycan indicating the 3,4-peptide crosslinks formed by D,D-transpeptidases and the 3,3-peptide crosslinks dominating in *M. tuberculosis* cell wall, formed by L,D-transpeptidases. NAG, *N*-acetylglycosamine; NAM, *N*-acetylmuramic acid.

(C) Synthesis of monocyclic β-lactams selected for this study. Reagents and conditions: (a) R′S-SR, SO_2Cl_2, TEA, CH_2Cl_2, 0°C, then reflux, 4 h; yields of isolated compounds after flash chromatography are reported in parentheses in (D).

(D) *N*-Thio-β-lactams produced for this study.

units and short tetra- or pentapeptide stems attached to the *N*-acetylmuramic acid moieties that form crosslinks with adjacent peptides. The polymer character of PG and consequent cell wall stability are reliant on the integrity and density of these peptide crosslinks (Vollmer et al., 2008). The unique features of the *M. tuberculosis* PG are the *N*-glycolylmuramic acid building blocks in the glycan chains and the unusual peptide crosslinks. The sequence of the tetrapeptide stems is the conventional found in most eubacteria (Figure 1B); however, the carboxylates in D-Glu and *meso*-Dap residues are amidated and the crosslinking pattern is distinctive. The conventional peptide crosslinks in most eubacteria are the Dap-Ala, so-called 3,4 crosslinks; *M. tuberculosis* peptidoglycan instead contains a high density (up to 80%) of Dap-Dap crosslinks (so-called 3,3 crosslinks, Figure 1B). This crosslinking pattern is dominant in the intra-macrophage state, suggesting its importance for intra-host survival and infectivity of the pathogen (Jankute et al., 2015; Maitra et al., 2019; Kumar et al., 2012; Lavollay et al., 2008). These 3,3 crosslinks are produced by the L,D-transpeptidases (Figure S1) that are not related to the D,D-transpeptidases, the classical penicillin-binding proteins, which produce the conventional 3,4 linkages (Vollmer et al., 2008; Mainardi et al., 2005). Five L,D-transpeptidases (Ldt) are found in the *M. tuberculosis* H37Rv genome, and among them Ldt_{Mt2} (Rv2518c) exhibits the highest expression level and was shown to be essential for infectivity in the mouse model of TB (Gupta et al., 2010). Ldt_{Mt2} is a validated target based on studies ranging from genetics, biochemistry, and infection models consistent with the observed phenotypes of the Ldt_{Mt2} knockout strains (Gupta et al., 2010; Schoonmaker et al., 2014; Sanders et al., 2014). Chemical validation relies on the fact that Ldt_{Mt2} is the target of meropenem, being the reason for meropenem sensitivity (Wivagg et al., 2016). The remarkable bactericidal effect of the meropenem-clavulanate (a BLA inhibitor) combination was observed on dormant mycobacteria and drug-resistant strains, and in the mouse TB model (Xiong et al., 2013; England et al., 2012; Dauby et al., 2011). Moreover, the combination was successfully used in the clinical treatment of extensively drug-resistant tuberculosis (De Lorenzo et al., 2013; Payen et al., 2012). These collective facts bring Ldt_{Mt2} and β-lactam antibiotics in focus for future TB therapy. The covalent adduct formation between the active-site cysteine of Ldt_{Mt2} and β-lactam type antibiotics (penam, penem, and carbapenem class, Figure 1A) was shown by us and by others (Cordillot et al., 2013; Steiner et al., 2017; Kumar et al., 2017; Iannazzo et al., 2016; Wang et al., 2020), and it was established that the penem-type β-lactam, faropenem, is the most effective on Ldt_{Mt2} as target (Steiner et al., 2017).

Faropenem was the most successful β-lactam even in the absence of clavulanate in killing *M. tuberculosis* in *in vitro* cultures and inside macrophages (Dhar et al., 2015). Mass spectrometry and structural and biochemical analysis shed light on the mechanism of faropenem action on Ldt_{Mt2}. Following the nucleophilic attack by the active-site cysteine on the lactam ring of faropenem, the primary adduct decomposes, leaving a small 86-Da fragment of the antibiotic (285 Da) attached to the cysteine in the active site, thus locking the enzyme in a

non-reactive, dead-end complex (Steiner et al., 2017; Kumar et al., 2017). The detailed mechanism of adduct evolution was described recently (Lohans et al., 2018, 2019); additionally it was revealed that faropenem follows a classical mechanism without decomposition after acyl-enzyme adduct formation when targeting the D,D-transpeptidase PBP3 (Lu et al., 2020). These recent achievements suggest that the inhibition of peptidoglycan biosynthesis by β-lactam antibiotics following the faropenem-type mechanism of action holds a potential for future TB therapy with Ldt_{Mt2} as the target in focus (Wivagg et al., 2014; Steiner et al., 2017; Kumar et al., 2017; Dhar et al., 2015; Tiberi et al., 2019).

Turos and co-workers reported the synthesis and biological evaluation of monocyclic β-lactams with an alkylthio group on the lactam nitrogen atom with antibacterial activity against *Bacillus* and *Staphylococcus* species (Turos et al., 2000, 2002). The presence of an *N*-methylthio group was essential for activity against methicillin-resistant *Staphylococcus aureus* strains isolated from pediatric patients with cystic fibrosis (Galletti et al., 2011; Cervellati et al., 2013; Giacomini et al., 2017a; Martelli and Giacomini, 2018). *M. tuberculosis* was moderately affected by these *N*-thio-β-lactams, or even by compounds with the sulfur linked on the C-4 position of the β-lactam ring (Bhattacharya and Turos, 2012; Majewski et al., 2016; Kostova et al., 2011). Concerning the mechanism of the antibacterial activity, it was proposed that the bacteriostatic effect of *N*-thio-lactams is mediated by different mechanism than that of the classical β-lactams (Revell et al., 2007).

A series of monocyclic β-lactams (Figures 1C and 1D) were designed, synthesized, and evaluated in this study against Ldt_{Mt2} as the target from *M. tuberculosis*. These novel *N*-thio-β-lactams were found to form covalent adducts at the Ldt_{Mt2} active site. Kinetic studies following the rate of adduct formation were used to identify the most effective compounds and confirmed the high stability of the modified state of the target protein. Data from mass spectrometry and X-ray crystallography consistently point at the formation of a mixed disulfide adduct at Cys354. Selected compounds were finally evaluated on *M. tuberculosis in vitro* to demonstrate their antimycobacterial activity on drug-susceptible and MDR clinical isolates.

RESULTS AND DISCUSSION

Design and synthesis of *N*-thio-substituted monocyclic β-lactam compounds

Faropenem, the most effective β-lactam-type inhibitor of Ldt_{Mt2} to date, forms a small covalent adduct at the active-site cysteine, thus suggesting that other β-lactam compounds following a similar mechanism or leading to the formation of small adducts may be useful candidates against this target. A series of 12 *N*-alkylthio- and *N*-arylthio-azetidinones were designed and synthesized for this study (Figures 1C and 1D). With respect to an already reported procedure (Galletti et al., 2011), a new variant of the *N*-thiolation procedure was studied and applied here for the synthesis of the compounds. The optimized procedure made use of the selected disulfide in the presence of sulfuryl chloride and triethylamine (TEA) in dichloromethane (Figure 1C) (Giacomini et al., 2017b). The milder reaction conditions afforded crudes that are purified by flash chromatography, as already reported for the synthesis of compounds **1a** and **2a**. Employing the same methodology, starting from the commercially available compounds **1** and **2**, the uncharacterized β-lactams **1b** to **1g** and **2b** to **2e** were obtained with a purity >95% and fully characterized (see STAR Methods and Data S1).

Covalent adduct formation at the Ldt_{Mt2} active site

To evaluate the panel of monocyclic compounds on the *M. tuberculosis* Ldt_{Mt2} as target and to identify the compounds leading to the formation of a stable covalent adduct at the active site, we employed the spectrophotometric dithio-nitrobenzoate (DTNB)-based assay (Figure 2A). The two-domain protein construct (BC module) derived from Ldt_{Mt2} contains a single cysteine residue, the active-site Cys354, which forms covalent adducts with β-lactam compounds. The structure of the this two-domain fragment (BC module) comprising an immunoglobulin-like domain (B) and the catalytic domain (C) does not show significant differences when compared with the complete periplasmic fragment of the enzyme comprising three domains (A, B, and C). The superposition of the BC module from the full-length protein including the residue range 55–408 (PDB: 3VYN; Li et al., 2013) and the isolated BC module gives C_α root-mean-square deviation of 0.79 Å; moreover, the active-site residues are in the same position and adapt the same conformation (Figure S1). Adduct formation by the active-site cysteine residue as a consequence of β-lactam exposure hinders the DTNB-dependent thiol derivatization and hence the concomitant stoichiometric thionitrobenzoate (TNB; A_{max} at 412 nm) release (Figure 2A). Meropenem, which forms a well characterized and stable adduct (Steiner et al., 2017; Kim et al., 2013), was used as a positive control while the protein with no compound exposure was used as negative control (Figure 2B).

The DTNB-based assay was employed to test the set of 12 monobactams at a single concentration (1.0 mM) to detect the adduct formation ability at the active site of the target protein. Higher spectrophotometric signals for **2a**, **2b**, **2c**, **2d**, **2e**, **1d**, and **1f** indicated no adduct formation or unstable adduct (Figure 2B). On the other hand, compounds **1a**, **1b**, **1c**, **1e**, and **1g** resulted in lower signals similar to that of the control compound meropenem, blocking the active-site cysteine and indicating a fast and stable adduct formation (Figure 2B). The series containing the bulky OTBS moiety (**2a**, **2b**, **2c**, **2d**, **2e**) or the larger *N*-thio-substituent (**1f**) were less successful in adduct formation. The reason is most likely that bulky groups do not allow compound docking at the enzyme active site in a position favoring nucleophilic attack by Cys354. Thus, β-lactams **1a**, **1b**, **1c**, **1e**, and **1g** were further investigated by kinetic measurements and for adduct stabilization in biochemical assays and mass spectrometry. The time-resolved sampling of the protein-monobactam reaction mixtures containing 50 μM protein and 50 μM compound subjected to DTNB derivatization were utilized to record the kinetics of the adduct formation (Figure 2C). The rate constants k_{obs} of the adduct formation were derived from exponential fits for the tested compounds and for meropenem as comparison. The kinetic constants were used to rank the compounds as **1b** > **1c** > **1g** = **1e** > **1a**, since the fast adduct formation is the prerequisite of an effective

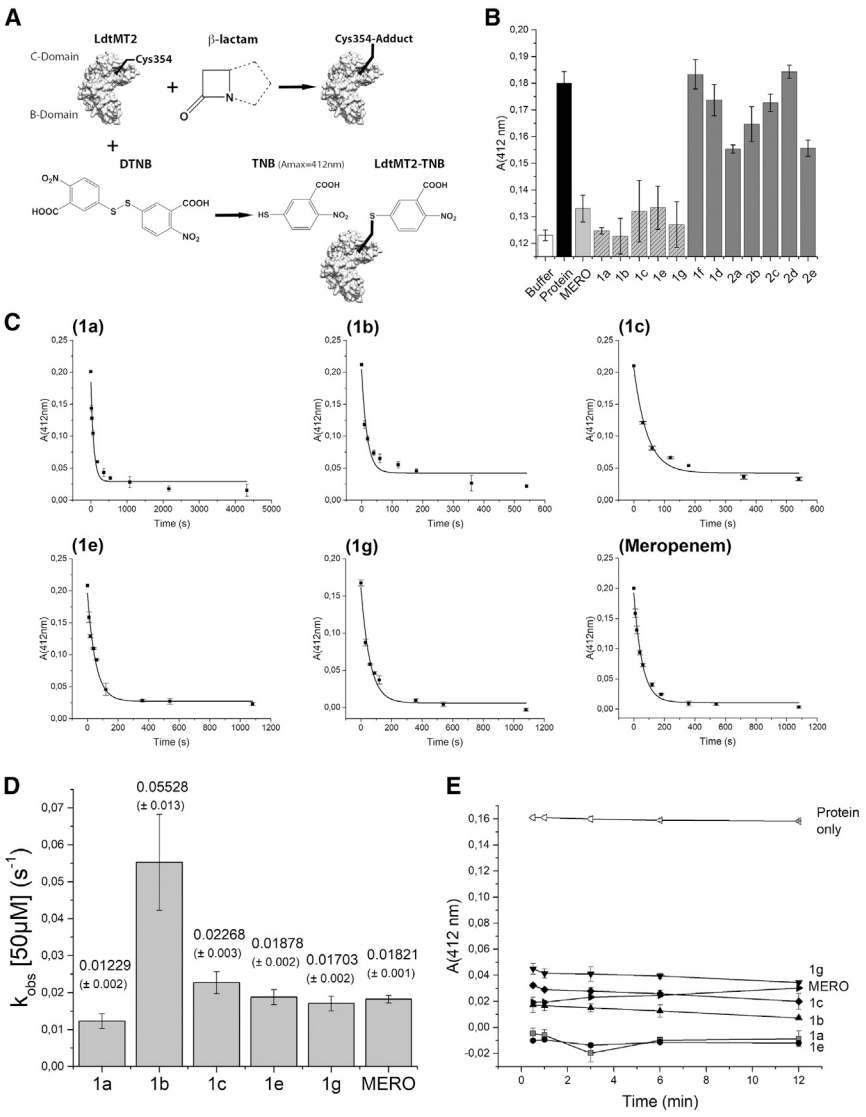

Figure 2. Kinetic analysis of adduct formation at the Ldt_{Mt2} active site

(A) Principle of the DTNB-based assay to monitor β-lactam dependent adduct formation. The active-site Cys354 derivatization by DTNB and the concomitant release of a TNB (A_{max}: 412 nm) molecule produces a spectrophotometric signal. Blocking the active-site Cys354 by a β-lactam-derived adduct does not allow DTNB derivatization and TNB release, hence the A_{412} signal is low.

(B) Screening for adduct formation by the DTNB assay. A_{412} values for the control samples and for the samples after compound exposure are shown from triplicate measurements; error bars indicate the standard deviation. MERO, meropenem (used as positive control).

(C) Kinetics of adduct formation for the five potent compounds and meropenem for comparison. Mean A_{412} values from triplicate measurements at various time points plotted against time and used to fit an exponential (solid line) to derive the rate constants k_{obs} for each compound.

(D) Comparison of the rate constants (k_{obs}) for the five potent compounds. The mean k_{obs} values from triplicate measurement and the standard error is indicated above the bars for each compound.

(E) Adduct stability for the five adducts (**1a**, **1b**, **1c**, **1e**, **1g**) and for the meropenem-derived adduct in the presence of *meso*-Dap; the potential acceptor substrate is followed. A_{412} values were recorded in triplicate, and error bars indicate standard error.

inhibition in the case of covalent inhibitors. The rate of adduct formation of carbapenems (meropenem, doripenem, and ertapenem) are in the range of 0.011–0.018 s^{-1} on the same protein target Ldt_{Mt2} under comparable conditions (Steiner et al., 2017). Hence **1g**, **1c**, and **1e** are approximately as potent in covalent adduct formation as these carbapenems or meropenem as demonstrated here, while **1b** shows faster binding kinetics (Figure 2D).

During the catalytic cycle of Ldt_{Mt2} the covalently bound donor peptide stem (acyl-enzyme intermediate) would react with the amino group of the Dap moiety from the acceptor peptide stem, leading to the formation of a new peptide bond, regenerating the ground-state enzyme with a free sulfhydryl at Cys354 (Figure S1). Since the acyl-enzyme adducts derived from the classical β-lactams resemble the reaction intermediate (Steiner et al., 2017; Kumar et al., 2017), the acceptor substrate may react with it, releasing the free Cys354 in the active site. The process as described above would lead to the release of the ground-state enzyme (Figure S1) and to a signal measurable by the DTNB assay. The preformed protein adducts derived from the five compounds **1a**, **1b**, **1c**, **1e**, and **1g** and meropenem were challenged by *meso*-diaminopimelate (*meso*-Dap), a potential substrate that may act as acceptor in the second half-reaction of the transpeptidase catalytic cycle (Figure S1). In this kinetic screen the absorbance (A_{412}) remained close to the initial values in each case and no adduct release was observed (Figure 2E). These results confirm that the adduct-modified state represents a blocked and dead-end state of the transpeptidase.

Mass spectrometric detection of adduct formation at the Ldt_{Mt2} active site

The protein samples exposed to the monocyclic compounds were analyzed by nano-electrospray ionization mass spectrometry to determine the mass of the covalent protein-compound adducts. The mass of the protein is instrumentally detected as 28,490 Da, 6 Da higher than the mass calculated from the protein sequence (28,484 Da). From samples with compound exposure, typically a single mass unique for each compound could be detected (Figure 3A and Table 1). The Cys354Ala mutant variant of the protein construct did not form the covalent adduct, hence the unmodified protein mass 28,450 ± 2.1 Da (Figure 3B) could be detected, confirming the site of adduct formation as the active-site Cys354. The mass difference in the samples as a consequence of compound exposure indicated the formation of

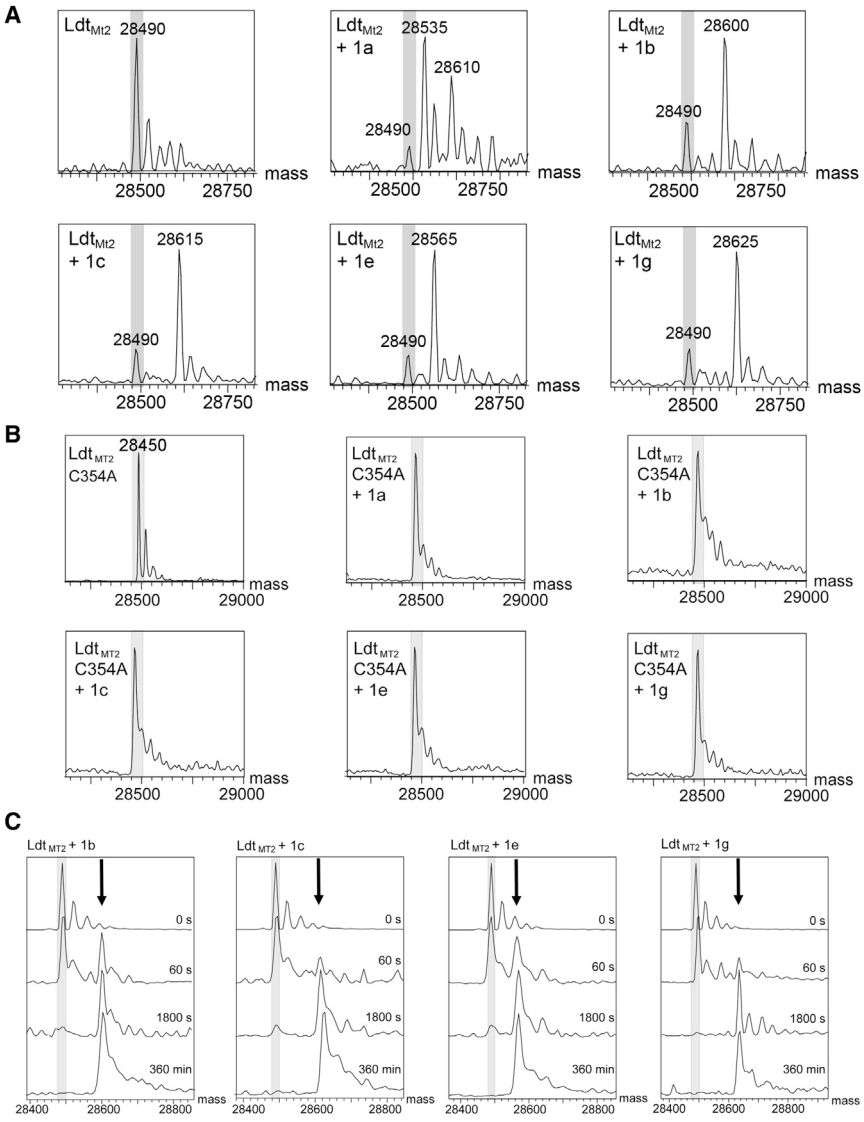

Figure 3. Mass spectrometric analysis of covalent adduct formation

(A) Mass spectra of Ldt_{Mt2} and adducts of Ldt_{Mt2} with the compounds **1a**, **1b**, **1c**, **1e**, and **1g**. The mass corresponding to the unmodified target protein (28,490 Da) is indicated by the gray bar. The extra masses as a consequence of compound exposure are indicated by the numbers above the peaks.

(B) Mass spectra of C354A mutant variant of Ldt_{Mt2} and the spectra after exposure to the compounds **1a**, **1b**, **1c**, **1e**, and **1g**. The mass corresponding to the unmodified target protein detected as 28,450 Da is indicated by the gray bar.

(C) Adduct stability indicated by the time-resolved sampling of the reactions for the most potent covalent inhibitors **1b**, **1c**, **1e**, and **1g** at 0 s, 60 s, 1,800 s, and 360 min time points. The gray bar indicates the peak of the unmodified protein mass, and the arrows indicate the peak corresponding to the protein-adduct mass.

covalent adducts, although this additional mass was never the full molecular weight of the compound but a lower mass, indicating that only a small fragment of the compound was bound.

The delta-mass values were consistent with the covalent attachment of the -S-R′ substituent present in the cases of each compound (Table 1). This result was intriguing, since the covalent adducts derived from bicyclic β-lactam compounds, such as the carbapenems previously studied (Cordillot et al., 2013; Steiner et al., 2017; Kumar et al., 2017), were linked via the carbonyl group after a β-lactam ring-opening reaction. Here the mass spectrometry data indicated that these *N*-thio-β-lactams behaved differently, forming the adduct with the thio group instead of lactam ring opening (Table 1).

The lifetime of these modified states was tested by sampling the nearly equimolar mixtures of protein (40 μM) and compound (50 μM) in the 0- to 360-min range (Figure 3C). In this setup a complete derivatization is achieved; however, prospective adduct hydrolysis would regenerate the native unmodified protein since a secondary adduct formation would not be possible. On exposing Ldt_{Mt2} to compounds **1b**, **1c**, **1e**, and **1g**, the resulting adducts could be detected without degradation even after 360 min (Figure 3C). The high stability of these adducts indicates a long-term inactivation of the target protein in line with data from kinetic analysis (Figures 2C and 2E). The compounds with larger substituent **1d** and **1f** formed an adduct with the transfer of their respective S-R′ moiety (Table 1), but their action was not kinetically favored (Figure 2B).

To demonstrate that an intact catalytic site would be responsible for the nucleophilic attack to the *N*-thio-β-lactams, we tested protein samples denatured prior to compound exposure. In all cases none of the compounds formed adducts, indicating that the *N*-thio-β-lactam action requires the folded protein and these compounds are suicide inhibitors of the Ldt_{Mt2} transpeptidase.

Structures of the protein-adduct complexes reveal the nature of the adducts

Since the mass spectrometry data indicated unexpected adduct formation with the potent *N*-thio-β-lactam compounds, further investigation was initiated to obtain structural information about the adduct-blocked state of Ldt_{Mt2}. The structures of the protein-adduct complexes in the cases of **1b** and **1g** were determined from X-ray diffraction data to 1.45-Å and 1.85-Å resolution, respectively, by crystallizing the preformed protein-adduct complexes. For **1a**, **1c**, and **1e** the corresponding adducts were obtained in crystalline state by soaking the preformed protein crystals with the compounds, and the structures of the corresponding complexes were determined to 1.77 Å resolution for **1a** and **1c** and to 1.65-Å resolution for **1e**. X-ray diffraction data statistics and model parameters are presented in Table S1. The

Table 1. Mass values derived from the mass spectra of Ldt_{M2} (BC-mod) reacted with the *N*-thio-β-lactam compounds 1a to 1g

Case tested	*N*-Thio-β-lactam mass (Da)	Mass detected (Da)	Δ*m* (Da)	Conclusion
Ldt_{Mt2}, 28,484 Da	–	28,490	6	native protein mass (+6 Da)
Ldt_{Mt2} + **1a**	**1a** (175)	28,535 (native: 28,490)	45	protein adduct with the fragment *S*-methyl (47 Da)
Ldt_{Mt2} + **1b**	**1b** (237)	28,600 (native: 28,490)	110	protein adduct with the fragment *S*-Ph (109 Da)
Ldt_{Mt2} + **1c**	**1c** (251)	28,615 (native: 28,490)	125	protein adduct with the fragment *S*-CH_2Ph (123 Da)
Ldt_{Mt2} + **1d**	**1d** (203)	28,565 (native: 28,490)	75	protein adduct with the fragment *S*-*iso*propyl (75 Da)
Ldt_{Mt2} + **1e**	**1e** (203)	28,565 (native: 28,490)	75	protein adduct with the fragment *S*-propyl (75 Da)
Ldt_{Mt2} + **1f**	**1f** (294)	28,655 (native: 28,490)	165	protein adduct with the fragment *S*-benzothiazolyl (166 Da)
Ldt_{Mt2} + **1g**	**1g** (267)	28,625 (native: 28,490)	135	protein adduct with the fragment *S*-*p*OMePh (139 Da)

Delta-mass values (Δ*m*) were derived using the native protein mass detected in the same spectra.

structures were solved by molecular replacement using the solvent and ligand free coordinates of the Ldt_{Mt2} BC module (Böth et al., 2013). The crystals belong to the $P2_1$ crystal form harboring two polypeptide chains in the crystal asymmetric unit (ASU) in essentially identical conformations with ordered residues at the active-site cleft and in the mobile lid domain covering the active site (Figure 4A). The only disordered region was observed in the structure of the **1a**-derived adduct at the tip of the lid module including a three-residues-long segment (residues 308–310). The Ldt_{Mt2} catalytic site is situated on a β-sheet platform presenting the catalytic dyad (Cys354, His336) under the mobile lid module comprising residues 303–323. This β-hairpin module can adopt various conformations ranging from wide-open as observed in the TNB adduct (PDB: 5LB1), half-open as observed in the meropenem-adduct structure (PDB: 4GSU), or closed as in the faropenem-derived adduct (PDB: 5LBG) and the native protein (PDB: 4HUC) (Steiner et al., 2017; Kim et al., 2013; Böth et al., 2013). The lid domain in the current protein complexes derived from **1a**, **1b**, **1c**, **1e**, and **1g** adopted a closed conformation similar to that observed in faropenem-derived adduct and in the native structure of the protein (Figure 4B).

The electron density maps (Figure 4C) revealed modification of the cysteine residue in the active site and allowed modeling of the covalent adducts consistent with the mass differences derived from mass spectrometry data presenting the moieties derived from the *N*-thio-β-lactams **1a**, **1b**, **1c**, **1e**, and **1g** (Table 1). The adducts are bound to Cys354 as mixed disulfides with S–S bond distances in the range of 2.05–2.09 Å in the refined structures, perfectly matching the S–S bond distances present in high-resolution protein structures (2.05–2.20 Å). The adduct residues display B factors in the range of that of the surrounding amino acid side chains. The two adducts that were formed in solution prior to crystallization, derived from **1b** (phenylthio residue) and **1g** (*p*-methoxy-phenylthio adduct), bound in a manner similar to that of mixed disulfide to Cys354 in both protein chains of the asymmetric unit. The remaining three adduct-bound states produced by crystal soaking present different occupancy in the two protein chains of the ASU. The methylthio adduct originating from **1a** is present in both chains, although in one of the chains its occupancy is clearly lower. Therefore, it was modeled with full occupancy in one of the protein chains of the ASU and at 50% occupancy in the other. The propylthio adduct derived from **1e** bound in one of the two protein chains only. The benzylthio residue originating from **1c** is bound in one of the polypeptide chains of the ASU, likely exhibiting multiple conformations, and was modeled at 50% occupancy in the dominant conformation.

The variation of the adduct occupancy between the two protein chains of the ASU occurs in the structures where the complexes were formed by crystal soaking, and this phenomenon reflects the difference in accessibility of the two active sites via the solvent channels of the protein crystal in this $P2_1$ crystal form. The interactions and solvent accessibility of these covalent ligands were analyzed in both chains constituting the ASU where applicable (Table S2). The adduct moieties derived from **1a**, **1c**, and **1e** adopt a conformation similar to that of the faropenem-derived β-hydroxy-butyryl adduct, while the ones originating from **1b** and **1g** are aligned in a different manner (Figure S2).

The hydrophobic adduct moieties (Figure 4C) are caged by the residues surrounding the catalytic dyad of the Ldt_{Mt2} of the dominantly hydrophobic binding site formed by the side chains of Met303, Tyr318, Thr320, Val322, Val331, Phe332, and Trp340 (Figures 4D and S3). The two conformations representing the two distinct binding modes of these modifications are shown in Figure 4D using the structures from **1e**- and **1g**-derived protein adducts as examples. No hydrogen bonding or polar interactions are present; the adduct fragments originating in **1b** and **1g** fill the hydrophobic cage and display the typical van der Waals distances of 3.2–3.4 Å. The adduct moieties derived from **1a**, **1c**, and **1e** adopt a different orientation (Figures 4D, S2, and S3) and also display slightly larger intermolecular distances in the range of 3.4–3.7 Å from the side chains of the active-site cleft.

An important feature of the *N*-thio-β-lactam-derived adducts revealed by the five X-ray structures is the closed conformation (Figure 4B). The solvent-accessible surface areas (SASA) of the Sγ of Cys354 or that of the adduct S atoms are small, accounting for 0–5 $Å^2$ (Table S2). The differences in SASA when comparing two chains of the ASU in the cases of **1a**, **1b**, and **1g** adducts reflect the small differences in conformations of the surrounding amino acid side chains. The low solvent exposure does not promote external attack on these adducts leading to potential hydrolysis, and supports the stability and long lifetime of the inactivated state. Moreover, the extended active-site modification in the current structures with the covalent modifications derived from **1a**, **1c**, and **1e** also blocks the binding pocket of the

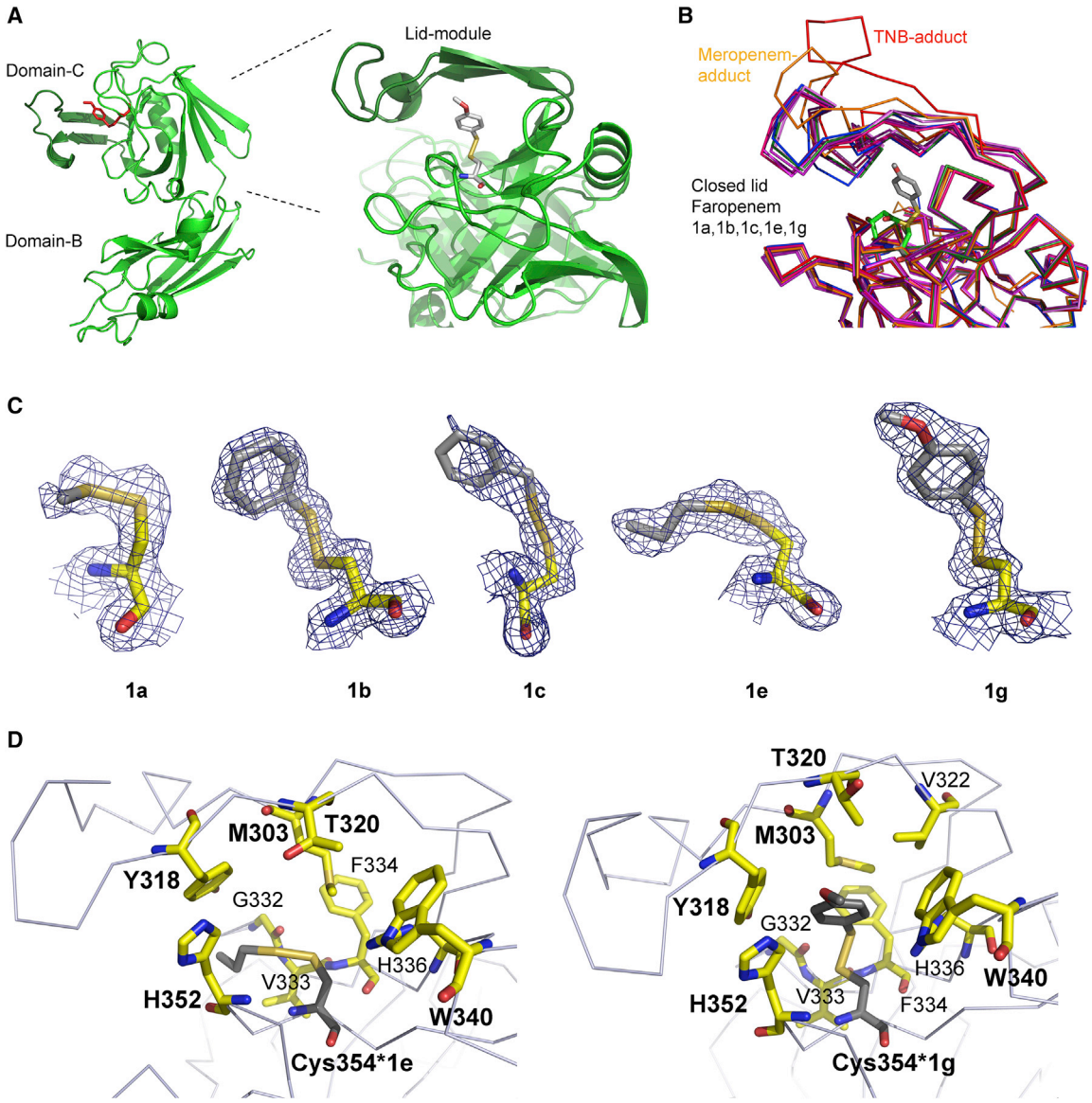

Figure 4. Structures of the Ldt_{Mt2} with the covalent adducts derived from *N*-thio-β-lactams

(A) Overall structure of the Ldt_{Mt2} BC module is depicted as green cartoon. In the close-up image, the covalent modification of the active-site Cys354 located in the catalytic domain (Domain-C) under the lid module is illustrated by the adduct derived from **1g**, and shown as stick model (gray carbons).

(B) Cα backbone of the various adduct-bound structures of Ldt_{Mt2}, illustrating the open (red, TNB adduct, PDB: 5LB1), the intermediate (orange, meropenem adduct, PDB: 4GUS), or the closed (green, faropenem adduct, PDB: 5LB1) conformation; the Cα backbone traces of the enzyme with the adducts originating from **1a**, **1b**, **1c**, **1e**, and **1g** are depicted in the shades of magenta and blue. The faropenem-derived and **1g**-derived adducts are represented as stick model in green and gray, respectively.

(C) $2F_o$-F_c electron density maps shown as a blue mesh at the position of the adduct-modified Cys354 residues contoured at 1.0σ. The modified Cys354 and the covalent modifications originating in the various *N*-thio-β-lactams are depicted as sticks with yellow and gray carbons, respectively.

(D) Binding site of the adducts derived from **1e** (left) and **1g** (right). The Ldt_{Mt2} Cα trace is shown as gray ribbon, the modified Cys354 as stick model with gray carbons, and the surrounding residues constituting the binding site as yellow carbons.

acceptor substrate, similarly to the small β-hydroxy-butyryl adduct derived from faropenem (Figure S2).

The mechanism of adduct formation by *N*-thio-β-lactams

The active-site cysteine SH nucleophile may attack the *N*-thio-β-lactams in three positions. The attack on the carbonyl group causes a ring-opening reaction leading to the formation of a thioester adduct (Figure 5, path A), and represents the classical inhibition pathway of β-lactam antibiotics against bacterial transpeptidases. This mechanism of action is also observed on Ldt_{Mt2} in the cases of several β-lactams including meropenem and faropenem (Steiner et al., 2017; Kumar et al., 2017; Lohans et al., 2018, 2019; Kim et al., 2013). The attack of the Cys354-SH

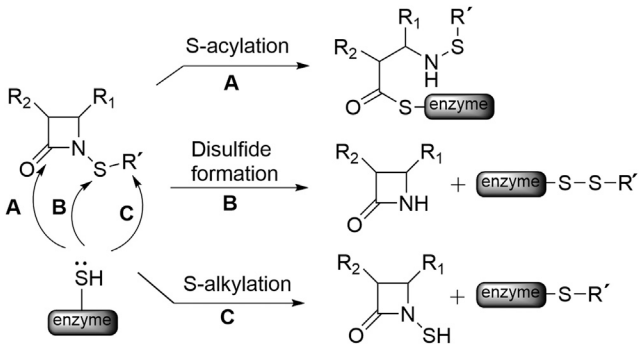

Figure 5. Potential nucleophilic attacks on *N*-thio-β-lactams by cysteine-dependent enzymes

S-Acylation (path A) is the conventional mode of action of β-lactam antibiotics leading to the acyl-enzyme adduct resembling the reaction intermediate of the catalytic cycle. The disulfide formation (path B) leads to a mixed disulfide adduct at the enzyme's active site as observed here in the case of the *N*-thio-β-lactam compounds (Figure 4). *S*-Alkylation (path C) is the energetically least favorable pathway and is not observed in this work.

nucleophile on the methyl group results in an alkylation reaction (Figure 5, path C); however, it is limited to more oxidized sulfur derivatives such as dimethylsulfate (Smith and March, 2007). Alternatively, the Cys354-SH nucleophile attacks the sulfur atom, leading to a mixed disulfide adduct (Figure 5, path B); this path involves the breaking of the weakest N–S bond (111 kcal/mol) compared with C–N (184 kcal/mol, path A) or C–S (167 kcal/mol, path B) (Rumble, 2020). Moreover, following the hard and soft concepts, a soft -SH nucleophile such as a cysteine-dependent enzyme can obtain more favorable interactions with a soft electrophile such as the methylthioether, and therefore the disulfide bond formation is preferred (Anslyn and Dougherty, 2006), as observed here in the case of the reaction between the *N*-thio-β-lactams and Ldt_{Mt2}.

The structural analysis and the results from mass spectrometry are consistent with path B (Figure 5) and the resulting mixed disulfide formation. A similar mechanism was reported for a different class of compounds, the isothiazolones, in the inhibition of the cysteine proteases cathepsin-B and histone acetyltransferase P300/CBP-associated factor (Wisastra et al., 2011). The transpeptidation reaction catalyzed by Ldt_{Mt2} initiates with a nucleophilic attack on the Dap carbonyl residue of the cell wall peptide stem, releasing the D-Ala residue (Figure S1). It is plausible that the docking of the *N*-thio-β-lactam would place its S group in a favorable arrangement for a nucleophilic attack by Cys354 in the active site. The resulting mixed disulfide is a stable modification and leads to an irreversible inactivation of the enzyme by blocking the catalytic machinery and occluding the substrate-binding cavity.

Antimycobacterial activity

The results from the kinetic investigation using the isolated Ldt_{Mt2} prompted us to test the efficacy of selected compounds for *in vitro* growth inhibition of *M. tuberculosis*. The *N*-thio-β-lactam compounds **1a**, **1b**, **1e**, **1g**, and **2a** were selected for preliminary testing for growth inhibition using a drug-susceptible clinical isolate of *M. tuberculosis*. The *N*-thio-β-lactams and reference drugs (isoniazid, rifampicin, ethambutol, and pyrazinamide) were tested at different concentrations in a drug susceptibility test (Table S3). Compounds **1e**, **1b**, and **1g** inhibited the growth of the drug-susceptible clinical isolate of *M. tuberculosis* at 20 μg/mL concentration.

In a second approach, the minimal inhibitory concentration (MIC) values were determined for the most active compounds **1b**, **1e**, and **1g** in the presence and absence of 5 μg/mL clavulanic acid against four *M. tuberculosis* strains: the reference strain H37Rv (ATCC 25618), a clinical isolate susceptible to first-line drugs, and two characterized MDR clinical isolates (MDR-1 and MDR-2), defined as resistant to rifampicin and isoniazid. The full characterization of drug susceptibility of the four MTB strains used in this study is shown in Table S4. Phenotypic results were confirmed by molecular tests (GenoType MTBDRplus and MTBDRsl).

The presence of clavulanic acid did not affect the MIC values (Table 2), thus suggesting that mycobacterial β-lactamases were not influencing the efficacy of these *N*-thio-β-lactams. Each compound (**1b**, **1e**, **1g**) presented an MIC of 10 μg/mL on the H37Rv reference strain and 20 μg/mL on the drug-susceptible clinical isolate. Compound **1e** was the most active toward the MDR clinical isolates, resulting in an MIC of 20 μg/mL on both isolates, while compound **1g** gave an MIC of 20 μg/mL and 40 μg/mL on the MDR-1 and MDR-2 strains, respectively (Table 2).

β-Lactam antimicrobial drugs have long been considered of limited use against *M. tuberculosis*, due to the rapid hydrolysis by broad-spectrum mycobacterial class-A β-lactamases (BlaC). Susceptibility testing of ampicillin, amoxicillin, and cephalosporins in the presence of clavulanic acid showed MIC values >16 μg/mL, which remains below the concentration achievable in serum (Abate and Miorner, 1998; Chambers et al., 1995). In contrast, a potent activity of meropenem-clavulanate combination was observed against susceptible and extensively drug-resistant strains (MIC <1 μg/mL) also in anaerobically grown culture (Hugonnet et al., 2009; De Lorenzo et al., 2013; Payen et al., 2012). The MIC values for meropenem and meropenem-clavulanate for the three stains used in this study were determined. The MIC for meropenem in the presence of clavulanate resulted in 32 μg/mL for H37Rv, 8 μg/mL for the drug-susceptible isolate, and 8 μg/mL for the two MDR isolates MDR-1 and MDR-2 (Table 2). These data are in agreement with literature data (Forsman et al., 2015; van Rijn et al., 2019).

The *in vitro* activity of meropenem-clavulanate is well established and indicates that the susceptibility of *M. tuberculosis* to this combination (MIC range 0.125–32 μg/mL) did not correlate with the resistance level to first-line or second-line antituberculosis drugs (Forsman et al., 2015; van Rijn et al., 2019). However, the difficulty of administering meropenem-clavulanate is a major obstacle to its adoption as an alternative therapy for TB. Instead faropenem, a stable and orally bioavailable β-lactam, has been shown to efficiently kill *M. tuberculosis* even in the absence of clavulanate, presenting an MIC value of 1.3 μg/mL (Dhar et al., 2015).

The *N*-thio-β-lactam compounds characterized here have an established mechanism of action on the validated β-lactam target Ldt_{Mt2}. One of the most effective compounds, **1e**, exhibited activity against drug-susceptible and also against

Table 2. Minimal inhibitory concentration values obtained against four *M. tuberculosis* strains: H37Rv (ATCC 25618), drug-susceptible, and two multidrug-resistant clinical isolates MDR-1 and MDR-2

		MIC (μg/mL)							
		H37Rv		Drug-susceptible		MDR-1		MDR-2	
Compound	[Comp] range (μg/mL)		Clav[b]		Clav[b]		Clav[b]		Clav[b]
1b[a]	1.25–40	10	10	20	20	≥40	≥40	≥40	≥40
1e[a]	1.25–40	10	10	20	20	20	20	20	20
1g[a]	1.25–40	10	10	20	20	20	20	40	40
Rifampicin[c]	0.12–16	≤0.12	NA	≤0.12	NA	≥16	NA	≥16	NA
Isoniazid[c]	0.03–4	≤0.03	NA	0.12	NA	≥4	NA	≥4	NA
Ethambutol[c]	0.5–32	4	NA	1	NA	32	NA	≥32	NA
Amikacin[c]	0.12–16	0.5	NA	0.25	NA	0.25	NA	≥16	NA
Meropenem[a]	0.12–64	≥64	32	≥64	8	≥64	8	≥64	8

MIC, minimal inhibitory concentration; NA, not available.
[a]MIC obtained in triplicate, resulting in the same value in each experiment.
[b]MIC values in the presence of 5 μg/mL clavulanic acid.
[c]MIC values obtained by MYCOTBI plate.

MDR isolates of *M. tuberculosis* with an MIC of 20 μg/mL (Table 2), suggesting that *N*-thio-β-lactams potentially represent candidates with established target-specific effect and mechanism of action for future antibiotic development against MDR TB.

SIGNIFICANCE

The monocyclic *N*-thio-β-lactam compounds developed and evaluated in this work target L,D-transpeptidase-2 (Ldt_{Mt2}), a validated target for antibiotic development from *Mycobacterium tuberculosis*. Single-turnover enzyme kinetic data showed that the best candidates are comparable or faster than meropenem and other carbapenems with regards to their binding kinetics when evaluated on the same molecular target Ldt_{Mt2}. Meropenem is the carbapenem currently in clinical trials assessing its potential for the treatment of pulmonary tuberculosis (https://clinicaltrials.gov/ct2/show/NCT02349841**). The kinetic and mass spectrometric analysis indicated covalent binding of a smaller fragment of the compounds at the active-site cysteine, Cys354 of the target protein. The adduct-mass values pointed at attachment of the alkylthio or aryl-thio moieties from the various *N*-thio-β-lactams. Five X-ray structures of the protein with the respective adducts bound revealed the nature of these covalent modifications. These *N*-thio-β-lactam compounds transferred their respective alkylthio or arylthio moieties onto Cys354, resulting in mixed disulfide adducts, thus not forming the conventional acylated derivatives as observed for traditional bicyclic β-lactam compounds studied earlier. The kinetic and mass spectrometric data consistently show that the adducts exhibit a long lifetime and suggest a long-term stable inactivation of the target protein. The five high-resolution X-ray structures revealed that these small fragments induce the closure of the active-site lid module, thus protecting the covalent modification and blocking the binding site of the substrate, further mitigating the stability of the dead-end complex. Two of the most active compounds showed growth inhibition in the μg/mL concentration range against *M. tuberculosis* strains in culture, including multidrug-resistant clinical isolates. Therefore, *N*-thio-β-lactams with established target-specific effect and mechanism of action potentially represent candidates for future antibiotic development against tuberculosis.**

STAR★METHODS

Detailed methods are provided in the online version of this paper and include the following:

- KEY RESOURCES TABLE
- RESOURCE AVAILABILITY
  - Lead contact
  - Materials availability
  - Data and code availability
  - Materials availability
- EXPERIMENTAL MODEL AND SUBJECT DETAILS
- METHOD DETAILS
  - Organic synthesis
  - Synthesis of N-thio-substituted-azetidinones
  - Protein production and purification
  - Adduct formation at the active site cysteine
  - Mass spectrometric analysis of covalent adduct formation
  - Protein crystallization and structure determination
  - Determination of antimycobacterial activity
- QUANTIFICATION AND STATISTICAL ANALYSIS

SUPPLEMENTAL INFORMATION

Supplemental information can be found online at https://doi.org/10.1016/j.chembiol.2021.03.008.

ACKNOWLEDGMENTS

D.G. would like to thank J. Monaldi and F. Molinari for technical assistance. This research was supported by the University of Bologna (RFO 2018 and

RFO 2019), Karolinska Institutet and Vinnova (Swedish Governmental Agency for Innovation, Grant Nr: 2017-00103). The authors would like to thank the financial support to T.B.P. from the CAPES (Coordenação de Aperfeiçoamento de Pessoal de Nível Superior - Brasil - Finance Code 001) and the support to C.C. from the COST Action CM1407. Special thanks are extended to the Protein Science Facility at Karolinska Institutet and to the beamline staff of the Biomax beamline at the MAX-IV synchrotron facility (Lund, Sweden).

AUTHOR CONTRIBUTIONS

D.G., R.S., E.M.S., and P.D.M. conceived and designed the experiments. G.M., M.C., and D.G. performed the organic syntheses and characterized the compounds. T.B.P., E.M.S., C.C., M.L., and R.S. performed the biochemical and structural analysis. F.B. and P.D.M. carried out the microbiological studies. D.G., R.S., and P.D.M. wrote the paper with contributions from all authors.

DECLARATION OF INTERESTS

The authors declare no competing interests.

Received: October 7, 2020
Revised: February 4, 2021
Accepted: March 12, 2021
Published: April 6, 2021

REFERENCES

Abate, G., and Miorner, H. (1998). Susceptibility of multidrug-resistant strains of *Mycobacterium tuberculosis* to amoxycillin in combination with clavulanic acid and ethambutol. J. Antimicrob. Chemother. *42*, 735–740.

Anslyn, E.V., and Dougherty, D.A. (2006). Modern Physical Organic Chemistry (University Science Books).

Bhattacharya, B., and Turos, E. (2012). Synthesis and biology of N-thiolated β-lactams. Tetrahedron *68*, 10665–10685.

Böth, D., Steiner, E.M., Stadler, D., Lindqvist, Y., Schnell, R., and Schneider, G. (2013). Structure of LdtMt2, an L,D-transpeptidase from *Mycobacterium tuberculosis*. Acta Crystallogr. D Biol. Crystallogr. *69*, 432–441.

Cervellati, R., Galletti, P., Greco, E., Cocuzza, C.E.A., Musumeci, R., Bardini, L., Paolucci, F., Pori, M., Soldati, R., and Giacomini, D. (2013). Monocyclic beta-lactams as antibacterial agents: facing antioxidant activity of N-methylthio-azetidinones. Eur. J. Med. Chem. *60*, 340–349.

Chambers, H.F., Moreau, D., Yajko, D., Miick, C., Wagner, C., Hackbarth, C., Kocagöz, S., Rosenberg, E., Hadley, W.K., and Nikaido, H. (1995). Can penicillins and other beta-lactam antibiotics be used to treat tuberculosis? Antimicrob. Agents Chemother. *39*, 2620–2624.

Cimarusti, C.M., and Sykes, R.B. (1984). Monocyclic beta-lactam antibiotics. Med. Res. Rev. *4*, 1–24.

Cordillot, M., Dubée, V., Triboulet, S., Dubost, L., Marie, A., Hugonnet, J.E., Arthur, M., and Mainardi, J.L. (2013). *In vitro* cross-linking of *Mycobacterium tuberculosis* peptidoglycan by L,D-transpeptidases and inactivation of these enzymes by carbapenems. Antimicrob. Agents Chemother. *57*, 5940–5945.

Dauby, N., Muylle, I., Mouchet, F., Sergysels, R., and Payen, M.C. (2011). Meropenem/clavulanate and linezolid treatment for extensively drug-resistant tuberculosis. Pediatr. Infect. Dis. J. *30*, 812–813.

Decuyper, L., Jukic, M., Sosic, I., Žula, A., D'hooghe, M., and Gobec, S. (2018). Antibacterial and β-lactamase inhibitory activity of monocyclic β-lactams. Med. Res. Rev. *38*, 426–503.

Dhar, N., Dubée, V., Ballell, L., Cuinet, G., Hugonnet, J.E., Signorino-Gelo, F., Barros, D., Arthur, M., and McKinney, J.D. (2015). Rapid cytolysis of *Mycobacterium tuberculosis* by faropenem, an orally bioavailable β-lactam antibiotic. Antimicrob. Agents Chemother. *59*, 1308–1319.

Diacon, A.H., van der Merwe, L., Barnard, M., von Groote-Bidlingmaier, F., Lange, C., García-Basteiro, A.L., Sevene, E., Ballell, L., and Barros-Aguirre, D. (2016). β-Lactams against tuberculosis—new trick for an old dog? N. Engl. J. Med. *375*, 393–394.

Dulberger, C.L., Rubin, E.J., and Boutte, C.C. (2020). The mycobacterial cell envelope—a moving target. Nat. Rev. Microbiol. *18*, 47–59.

Emsley, P., Lohkamp, B., Scott, W.G., and Cowtan, K. (2010). Features and development of Coot. Acta Crystallogr. D Biol. Crystallogr. *66*, 486–501.

England, K., Boshoff, H.I., Arora, K., Weiner, D., Dayao, E., Schimel, D., Via, L.E., and Barry, C.E., 3rd. (2012). Meropenem-clavulanic acid shows activity against *Mycobacterium tuberculosis in vivo*. Antimicrob. Agents Chemother. *56*, 3384–3387.

European Centre for Disease Prevention and Control (2018). Antimicrobial consumption. Annual epidemiological report for 2017. https://www.ecdc.europa.eu/en/publications-data/antimicrobial-consumption-annual-epidemiological-report-2017.

Forsman, L.D., Giske, C.G., Bruchfeld, J., Schön, T., Juréen, P., and Ängeby, K. (2015). Meropenem-clavulanic acid has high *in vitro* activity against multidrug-resistant *Mycobacterium tuberculosis*. Antimicrob. Agents Chemother. *59*, 3630–3632.

Galletti, P., and Giacomini, D. (2011). Monocyclic β-lactams: new structures for new biological activities. Curr. Med. Chem. *18*, 4265–4283.

Galletti, P., Cocuzza, C.E.A., Pori, M., Quintavalla, A., Musumeci, R., and Giacomini, D. (2011). Antibacterial agents and cystic fibrosis: synthesis and antimicrobial evaluation of a series of N-thiomethylazetidinones. Chem. Med. Chem. *6*, 1919–1927.

Giacomini, D., Musumeci, R., Galletti, P., Martelli, G., Assennato, L., Sacchetti, G., Guerrini, A., Calaresu, E., Martinelli, M., and Cocuzza, C. (2017a). 4-Alkyliden-azetidinones modified with plant derived polyphenols: antibacterial and antioxidant properties. Eur. J. Med. Chem. *140*, 604–614.

Giacomini, D., Torricelli, P., Gentilomi, G.A., Boanini, E., Gazzano, M., Bonvicini, F., Benetti, E., Soldati, R., Martelli, G., Rubini, K., et al. (2017b). Monocyclic β-lactams loaded on hydroxyapatite: new biomaterials with enhanced antibacterial activity against resistant strains. Sci. Rep. *7*, https://doi.org/10.1038/s41598-017-02943-2.

Gupta, R., Lavollay, M., Mainardi, J.L., Arthur, M., Bishai, W.R., and Lamichhane, G. (2010). The *Mycobacterium tuberculosis* protein LdtMt2 is a nonclassical transpeptidase required for virulence and resistance to amoxicillin. Nat. Med. *16*, 466–469.

Hall, L., Jude, K.P., Clark, S.L., Dionne, K., Merson, R., Boyer, A., Parrish, N.M., and Wengenack, N.L. (2012). Evaluation of the Sensititre MycoTB plate for susceptibility testing of the *Mycobacterium tuberculosis* complex against first- and second-line agents. J. Clin. Microbiol. *50*, 3732.

Hugonnet, J.E., Tremblay, L.W., Boshoff, H.I., Barry, C.E., 3rd., and Blanchard, J.S. (2009). Meropenem-clavulanate is effective against extensively drug-resistant *Mycobacterium tuberculosis*. Science *323*, 1215–1218.

Iannazzo, L., Soroka, D., Triboulet, S., Fonvielle, M., Compain, F., Dubée, V., Mainardi, J.L., Hugonnet, J.E., Braud, E., Arthur, M., and Etheve-Quelquejeu, M. (2016). Routes of synthesis of carbapenems for optimizing both the inactivation of L,D-transpeptidase LdtMt1 of *Mycobacterium tuberculosis* and the stability toward hydrolysis by β-lactamase BlaC. J. Med. Chem. *59*, 3427–3438.

Jankute, M., Cox, J.A., Harrison, J., and Besra, G.S. (2015). Assembly of the mycobacterial cell wall. Annu. Rev. Microbiol. *69*, 405–423.

Kabsch, W. (2010). XDS. Acta Crystallogr. D Biol. Crystallogr. *66*, 125–132.

Kim, H.S., Kim, J., Im, H.N., Yoon, J.Y., An, D.R., Yoon, H.J., Kim, J.Y., Min, H.K., Kim, S.J., Lee, J.Y., et al. (2013). Structural basis for the inhibition of *Mycobacterium tuberculosis* L,D-transpeptidase by meropenem, a drug effective against extensively drug-resistant strains. Acta Crystallogr. D Biol. Crystallogr. *69*, 420–431.

Kostova, M.B., Myers, C.J., Beck, T.N., Plotkin, B.J., Green, J.M., Boshoff, H.I., Barry, C.E., 3rd, Deschamps, J.R., and Konaklieva, M.I. (2011). C4-alkylthiols with activity against *Moraxella catarrhalis* and *Mycobacterium tuberculosis*. Bioorg. Med. Chem. *19*, 6842–6852.

Krissinel, E., and Henrick, K. (2007). Inference of macromolecular assemblies from crystalline state. J. Mol. Biol. *372*, 774–797.

Kumar, P., Arora, K., Lloyd, J.R., Lee, I.Y., Nair, V., Fischer, E., Boshoff, H.I., and Barry, C.E., 3rd. (2012). Meropenem inhibits D,D-carboxypeptidase activity in *Mycobacterium tuberculosis*. Mol. Microbiol. *86*, 367–381.

Kumar, P., Kaushik, A., Lloyd, E.P., Li, S.G., Mattoo, R., Ammerman, N.C., Bell, D.T., Perryman, A.L., Zandi, T.A., Ekins, S., et al. (2017). Non-classical transpeptidases yield insight into new antibacterials. Nat. Chem. Biol. *13*, 54–61.

Laskowski, R.A., and Swindells, M.B. (2011). LigPlot+: multiple ligand-protein interaction diagrams for drug discovery. J. Chem. Inf. Model. *51*, 2778–2786.

Lavollay, M., Arthur, M., Fourgeaud, M., Kumar, L., Marie, A., Veziris, N., Blanot, D., Gutmann, L., and Mainardi, J.L. (2008). The peptidoglycan of stationary-phase *Mycobacterium tuberculosis* predominantly contains cross-links generated by L,D-transpeptidation. J. Bacteriol. *190*, 4360–4366.

Li, W.J., Li, D.F., Hu, Y.L., Zhang, X.E., Bi, L.J., and Wang, D.C. (2013). Crystal structure of L,D-transpeptidase Ldt_{Mt2} in complex with meropenem reveals the mechanism of carbapenem against *Mycobacterium tuberculosis*. Cell Res. *23*, 728–731.

Li, F., Wan, L., Xiao, T., Liu, H., Jiang, Y., Zhao, X., Wang, R., and Wan, K. (2018). *In vitro* activity of β-lactams in combination with β-lactamase inhibitors against *Mycobacterium tuberculosis* clinical isolates. Biomed. Res. Int. *2018*, https://doi.org/10.1155/2018/3579832.

Lohans, C.T., van Groesen, E., Kumar, K., Tooke, C.L., Spencer, J., Paton, R.S., Brem, J., and Schofield, C.J. (2018). A new mechanism for β-lactamases: class D enzymes degrade 1β-methyl carbapenems through lactone formation. Angew. Chem. Int. Ed. *57*, 1282–1285.

Lohans, C.T., Chan, H.T.H., Malla, T.R., Kumar, K., Kamps, J.J.A.G., McArdle, D.J.B., van Groesen, E., de Munnik, M., Tooke, C.L., and Spencer, J. (2019). Non-hydrolytic β-lactam antibiotic fragmentation by L,D-transpeptidases and serine β-lactamase cysteine variants. Angew. Chem. Int. Ed. *58*, 1990–1994.

De Lorenzo, S., Alffenaar, J.W., Sotgiu, G., Centis, R., D'Ambrosio, L., Tiberi, S., Bolhuis, M.S., van Altena, R., Viggiani, P., Piana, A., et al. (2013). Efficacy and safety of meropenem–clavulanate added to linezolid-containing regimens in the treatment of MDR-/XDR-TB. Eur. Respir. J. *41*, 1386–1392.

Lu, Z., Wang, H., Zhang, A., Liu, X., Zhou, W., Yang, C., Guddat, L., Yang, H., Schofield, C.J., and Rao, Z. (2020). Structures of *Mycobacterium tuberculosis* penicillin-binding protein 3 in complex with five β-lactam antibiotics reveal mechanism of inactivation. Mol. Pharmacol. *7*, 287–294.

Mainardi, J.L., Fourgeaud, M., Hugonnet, J.E., Dubost, L., Brouard, J.P., Ouazzani, J., Rice, L.B., Gutmann, L., and Arthur, M. (2005). A Novel peptidoglycan cross-linking enzyme for a β-lactam-resistant transpeptidation pathway. J. Biol. Chem. *280*, 38146–38152.

Maitra, A., Munshi, T., Healy, J., Martin, L.T., Vollmer, W., Keep, N.H., and Bhakta, S. (2019). Cell wall peptidoglycan in *Mycobacterium tuberculosis*: an Achilles' heel for the TB-causing pathogen. FEMS Microbiol. Rev. *43*, 548–575.

Majewski, M.W., Watson, K.D., Cho, S., Miller, P.A., Franzblau, S.G., and Miller, M.J. (2016). Syntheses and biological evaluations of highly functionalized hydroxamate containing and N-methylthio monobactams as anti-tuberculosis and β-lactamase inhibitory agents. Med. Chem. Commun. *7*, 141–147.

Martelli, G., and Giacomini, D. (2018). Antibacterial and antioxidant activities for natural and synthetic dual-active compounds. Eur. J. Med. Chem. *5*, 158–191.

Murshudov, G.N., Skubák, P., Lebedev, A.A., Pannu, N.S., Steiner, R.A., Nicholls, R.A., Winn, M.D., Long, F., and Vagin, A.A. (2011). REFMAC5 for the refinement of macromolecular crystal structures. Acta Crystallogr. D Biol. Crystallogr. *67*, 355–367.

Payen, M.C., De Wit, S., Martin, C., Sergysels, R., Muylle, I., Van Laethem, Y., and Clumeck, N. (2012). Clinical use of the meropenem-clavulanate combination for extensively drug-resistant tuberculosis. Int. J. Tuberc. Lung Dis. *16*, 558–560.

Revell, K.D., Heldreth, B., Long, T.E., Jang, S., and Turos, E. (2007). N-thiolated beta-lactams: studies on the mode of action and identification of a primary cellular target in *Staphylococcus aureus*. Bioorg. Med. Chem. *15*, 2453–2467.

van Rijn, S.P., Zuur, M.A., Anthony, R., Wilffert, B., van Altena, R., Akkerman, O.W., de Lange, W.C.M., van der Werf, T.S., Kosterink, J.G.W., and Alffenaar, J.C. (2019). Evaluation of carbapenems for treatment of multi- and extensively drug-resistant *Mycobacterium tuberculosis*. Antimicrob. Agents Chemother. *63*. e01489–18. https://doi.org/10.1128/AAC.01489-18.

Rumble, J.R. (2020). CRC Handbook of Chemistry and Physics, 100th Ed. (CRC Press).

Sanders, A.N., Wright, L.F., and Pavelka, M.S., Jr. (2014). Genetic characterization of mycobacterial L,D-transpeptidases. Microbiology *160*, 1795–1806.

Schoonmaker, M.K., Bishai, W.R., and Lamichhane, G. (2014). Non-classical transpeptidases of *Mycobacterium tuberculosis* alter cell size, morphology, the cytosolic matrix, protein localization, virulence, and resistance to β-lactams. J. Bacteriol. *196*, 1394–1402.

Schüttelkopf, A.W., and van Aalten, D.M.F. (2004). PRODRG: a tool for high-throughput crystallography of protein-ligand complexes. Acta Crystallogr. *60*, 1355–1363.

Smith, M.B., and March, J. (2007). March's Advanced Organic Chemistry: Reactions, Mechanisms, and Structure, 6th Ed. (John Wiley & Sons, Inc). https://doi.org/10.1002/0470084960.

Steiner, E.M., Schneider, G., and Schnell, R. (2017). Binding and processing of β-lactam antibiotics by the transpeptidase LdtMt2 from *Mycobacterium tuberculosis*. FEBS J. *284*, 725–741.

Tacconelli, E., and Pezzani, M.D. (2019). Public health burden of antimicrobial resistance in Europe. Lancet Infect. Dis. *19*, 4–6.

Tacconelli, E., Carrara, E., Savoldi, A., Harbarth, S., Mendelson, M., Monnet, D.L., Pulcini, C., Kahlmeter, G., Kluytmans, J., Carmeli, Y., et al. (2018). WHO Pathogens Priority List Working Group. Discovery, research, and development of new antibiotics: the WHO priority list of antibiotic-resistant bacteria and tuberculosis. Lancet Infect. Dis. *18*, 318–327.

Tiberi, S., Zumla, A., and Migliori, G.B. (2019). Multidrug and extensively drug-resistant tuberculosis: epidemiology, clinical features, management and treatment. Infect. Dis. Clin. North Am. *33*, 1063–1085.

Turos, E., Konaklieva, M.I., Ren, R.X.F., Shi, H.C., Gonzalez, J., Dickey, S., and Lim, D.V. (2000). N-thiolated bicyclic and monocyclic β-lactams. Tetrahedron *56*, 5571–5578.

Turos, E., Long, T.E., Konaklieva, M.I., Coates, C., Shim, J.Y., Dickey, S., Lim, D.V., and Cannons, A. (2002). N-thiolated β-lactams: novel antibacterial agents for methicillin-resistant *Staphylococcus aureus*. Bioorg. Med. Chem. Lett. *12*, 2229–2231.

Vagin, A., and Teplyakov, A. (2010). Molecular replacement with MOLREP. Acta Crystallogr. D Biol. Crystallogr. *66*, 22–25.

Vollmer, W., Blanot, D., and de Pedro, M.A. (2008). Peptidoglycan structure and architecture. FEMS Microbiol. Rev. *32*, 149–167.

Wang, X., Gu, X., Zhang, C., Zhao, F., and Deng, K. (2020). Structural and biochemical analyses of the LdtMt2-panipenem adduct provide new insights into the effect of the 1-β-methyl group on carbapenems. Biochem. Biophys. Res. Commun. *523*, 6–9.

Wayne, P.A. (2018). Laboratory Detection and Identification of Mycobacteria, 2nd ed. (Clinical and Laboratory Standards Institute), CLSI guideline M48. https://clsi.org/standards/products/microbiology/documents/m48/.

Williams, C.J., Hintze, B.J., Headd, J.J., Moriarty, N.W., Chen, V.B., Jain, S., Prisant, M.G., Lewis, S.M., Videau, L.L., and Keedy, D.A. (2018). MolProbity: more and better reference data for improved all-atom structure validation. Protein Sci. *27*, 293–315.

Winn, M.D., Ballard, C.C., Cowtan, K.D., Dodson, E.J., Emsley, P., Evans, P.R., Keegan, R.M., Krissinel, E.B., Leslie, A.G.W., McCoy, A., et al. (2011). Overview of the CCP4 suite and current developments. Acta Crystallogr. D Biol. Crystallogr. *67*, 235–242.

Wisastra, R., Ghizzoni, M., Maarsingh, H., Minnaard, A.J., Haisma, H.J., and Dekker, F.J. (2011). Isothiazolones; thiol-reactive inhibitors of cysteine protease cathepsin b and histone acetyltransferase PCAF. Org. Biomol. Chem. *9*, 1817–1822.

Wivagg, C.N., Bhattacharyya, R.P., and Hung, D.T. (2014). Mechanisms of β-lactam killing and resistance in the context of *M. tuberculosis*. J. Antibiot. *67*, 645–654.

Wivagg, C.N., Wellington, S., Gomez, J.E., and Hung, D.T. (2016). Loss of a class a penicillin-binding protein alters β-lactam susceptibilities in *Mycobacterium tuberculosis*. ACS Infect. Dis. *2*, 104–110.

Xiong, X., Xu, Z., Yang, Z., Liu, Y., Wang, D., Dong, M., Parker, E.J.O., and Zhu, W. (2013). Key targets and relevant inhibitors for the drug discovery of tuberculosis. Curr. Drug Targets *14*, 676–699.

STAR★METHODS

KEY RESOURCES TABLE

REAGENT or RESOURCE	SOURCE	IDENTIFIER
Bacterial Strains		
Mycobacterium tuberculosis / strain H37Rv	ATCC	ATCC 25618
Mycobacterium tuberculosis (Susceptible)	Isolated from patient (this paper)	N/A
Mycobacterium tuberculosis Multidrug resistant MDR-1	Isolated from patient (this paper)	N/A
Mycobacterium tuberculosis Multidrug resistant MDR-2	Isolated from patient (this paper)	N/A
Escherichia coli / strain BL21(DE3), expression host	Merck	D48758
Recombinant Protein		
Ldt_{Mt2} BC-module, (including residues 149-408)	Own development, Böth et al., 2013.	n.a.
Deposited Data		
Ldt_{Mt2} BC-module / 1a-adduct structure at 1.77 Å	This paper	7A1C (wwPDB)
Ldt_{Mt2} BC-module / 1b-adduct structure at 1.45 Å	This paper	7A0Z (wwPDB)
Ldt_{Mt2} BC-module / 1c-adduct structure at 1.77 Å	This paper	7A1E (wwPDB)
Ldt_{Mt2} BC-module / 1e-adduct structure at 1.65 Å	This paper	7A11 (wwPDB)
Ldt_{Mt2} BC-module / 1g-adduct structure at 1.85 Å	This paper	7A10 (wwPDB)
LdtMt2 BC-module / Faropenem-derived adduct	Steiner et al., 2017	5LBG (wwPDB)
LdtMt2 BC-module / TNB-adduct	Steiner et al., 2017	5LB1 (wwPDB)
LdtMt2 BC-module / Meropenem-derived adduct	Kim et al., 2013	4GSU (wwPDB)
LdtMt2 BC-module	Böth et al., 2013	4HUC (wwPDB)
LdtMt2 3-domain structure (ABC)	Li et al., 2013	3VYN (wwPDB)
Recombinant DNA		
pNIC-LppS09	Böth et al., 2013.	n.a.
Software and Algorithms		
Origin / OriginLab (Northampton, Massachusetts, USA)	OriginLab	www.originlab.com
XDS	Kabsch 2010	http://xds.mpimf-heidelberg.mpg.de/
AIMLESS / CCP4i	Winn et al., 2011.	http://www.ccp4.ac.uk/download/
MOLREP / CCP4i	Vagin and Teplyakov 2010.	http://www.ccp4.ac.uk/download/
PRODRG	Schüttelkopf and van Aalten 2004	http://www.ccp4.ac.uk/download/
REFMAC / CCP4i	Murshudov et al., 2011	http://www.ccp4.ac.uk/download/
COOT	Emsley et al., 2010.	https://bernhardcl.github.io/coot/
PISA / CCP4i	Krissinel and Henrick 2007.	http://www.ccp4.ac.uk/download/
AREAIMOL / CCP4i	Winn et al., 2011	http://www.ccp4.ac.uk/download/
BAVERAGE / CCP4i	Winn et al., 2011	http://www.ccp4.ac.uk/download/
PyMOL	www.pymol.org	https://pymol.org/2/
LigPlot+	Laskowski and Swindells 2011	https://www.ebi.ac.uk/thornton-srv/software/LigPlus/download.html
MassLynx 4.1	www.waters.com	https://www.waters.com/waters/en_US/MassLynx-Mass-Spectrometry-Software-/nav.htm?cid=513164&locale=en_US
MolProbity	Williams et al., 2018	http://molprobity.biochem.duke.edu/
Epicenter	Becton Dickinson	https://www.bd.com/en-us/offerings/capabilities/microbiology-solutions/blood-culture/blood-culture-reporting-and-analytics/epicenter-microbiology-data-management-system

RESOURCE AVAILABILITY

Lead contact

Robert Schnell. E-mail: Robert.Schnell@ki.se.

Materials availability

The expression construct for the recombinant LdtMT2 construct used in this study will be made available on request, but we may require a completed Materials Transfer Agreement if there is potential for commercial application.

Data and code availability

The structure factors from the X-ray diffraction datastes and the refined models and are deposited with the Protein Data Bank (wwPDB at www.wwpdb.org) under Acc. Nr.: 7A1C, 7A0Z, 7A1E, 7A11, 7A10.

Materials availability

The clinical isolates of Mycobacterium tuberculosis will be made available for other scientists, upon request to the lead contact.

EXPERIMENTAL MODEL AND SUBJECT DETAILS

Mycobacterium tuberculosis strains used in this study

Mycobacterium tuberculosis H37Rv (ATCC 25618).

Mycobacterium tuberculosis clinical isolates used in this study were:

1) *Drug-susceptible strain*: It was susceptible to the following critical concentrations: 0.1μg/mL INH, 1 μg/mL RIF, 5 μg/mL EMB and 100 μg/mL PZA (obtained by the "gold standard" automatic Bactec MGIT 960 (MGIT, Becton Dickinson); No mutations were detected in the following genes: rpoB, katG inhA (obtained by GenoType MTBDRplus 2.0, Bruker, Germany)
2) *MDR-1strain*: It was resistant to the following critical concentrations: 0.4 μg/mL INH, 1 μg/mL RIF, 7.5 μg/mL EMB and 100 μg/mL PZA (obtained by the "gold standard" automatic Bactec MGIT 960 (MGIT, Becton Dickinson);

Mutations were detected in the following genes: *rpoB* (mut 3), *katG* (mut 1) (obtained by GenoType MTBDRplus 2.0, Bruker, Germany) and in *gyr A* (mut1) (obtained by GenoType MTBDRsl 2.0, Bruker, Germany)

3) *MDR-2 strain*: It was resistant to the following critical concentrations: 0.4 μg/mL INH, 1 μg/mL RIF, 7.5 μg/mL EMB and 100 μg/mL PZA (obtained by the "gold standard" automatic Bactec MGIT 960 (MGIT, Becton Dickinson);

Mutations were detected in the following genes: *rpoB* (mut 3), *katG* (mut 1) (obtained by GenoType MTBDRplus 2.0, Bruker, Germany) and in *rrs* (mut1) (obtained by GenoType MTBDRsl 2.0, Bruker, Germany)

The bacterial sample collection and documentation for this study was conducted in accordance with the Declaration of Helsinki.

For recombinant protein production *Escherichia coli* strain BL21(DE3) was utilized, available from Merck (Merck KGaA, Darmstadt, Germany) with genotype: F – *ompT hsd*SB (rB- mB-) *gal dcm* (DE3). The bacterial cultures were grown in Luria-Bertani media with the appropriate antibiotics (Kanamycine, 30 μg/ml) added, at 37°C or at 21°C as described in the method details section.

METHOD DETAILS

Organic synthesis

General procedures

Commercial reagents (reagent grade, >99%) and the commercially available azetidinones **1** and **2** were used as received (Sigma-Aldrich) without additional purification. Anhydrous solvents were obtained commercially from Sigma-Aldrich. All reactions were performed under an inert atmosphere (N_2). TLC: Merck 60 F_{254} plates. Column chromatography: Merck silica gel 200-300 mesh. ^{1}H and ^{13}C NMR spectra were recorded with an INOVA 400 instrument with a 5 mm probe. 2D NOESY experiments were run using 200 ms mixing time. All chemical shifts are quoted relative to deuterated solvent signals (δ in ppm and *J* in Hz). Polarimetric Analyses were conducted on Unipol L 1000 "Schmidt-Haensch" Polarimeter at 598 nm. FTIR spectra: Brucker instrument, measured as films between NaCl plates or CH_2Cl_2 solutions for solid compounds; wave numbers are reported in cm^{-1}. ATR-FTIR spectra: Alpha FT IR Bruker spectrometer with platinum ATR single reflection diamond module. As reference, the background spectrum of air was collected before the acquisition of each sample spectrum. Spectra were recorded with a resolution of 4 cm^{-1}, and 32 scans were averaged for each spectrum (scan range 4000–450 cm^{-1}). The purities of the target compounds were assessed as being >95% using HPLC-MS. HPLC-MS: Agilent Technologies HP1100 instrument, equipped with a ZOBRAX-Eclipse XDB-C8 Agilent Technologies column; mobile phase: H_2O/CH_3CN, 0.4 mL/min, gradient from 30 to 80% of CH_3CN in 8 min, 80% of CH_3CN until 25 min, coupled with an Agilent Technologies MSD1100 single-quadrupole mass spectrometer, full scan mode from m/z = 50 to 2600, in positive ion mode, ESI spray voltage 4500 V, nitrogen gas 35psi, drying gas flow 11.5mL/min, fragmentor voltage 20 V. High resolution mass: Waters Xevo G2-XS QTof , analyzer mode sensitivity, capillary voltage 3.00 kV, sample cone, 40 V, source temperature, 120°C, desolvation temperature: 600°C, Cone gas flow: 50 L h.

Synthesis of N-thio-substituted-azetidinones

Synthesis of azetidinones **1a**, **1b**, **2a** and **2b** were described and obtained with methods already reported (Galletti et al., 2011; Bhattacharya and Turos, 2012). ^{1}H and ^{13}C NMR spectra are presented in the supplemental information.

General procedure for the synthesis of thio-alkyl and thio-aryl β-lactams (GP1)

To a solution of the desired disulfide (1-1.25 equiv) in CH_2Cl_2 (2 mL) under inert atmosphere, a solution of SO_2Cl_2 (122 μL, 1.5 mmol, 1.5 equiv) in CH_2Cl_2 (2 mL) was added dropwise at 0°C. After 10 minutes, the desired azetidinone (1 mmol, 1 equiv) was introduced followed by the dropwise addition of TEA (277 μL, 2 mmol, 2 equiv). The mixture was stirred at reflux for 4 h, then cooled to room temperature, quenched with a saturated aqueous solution of NH_4Cl (5 mL) and extracted with CH_2Cl_2 (3 × 15 mL). The combined organic extracts were dried over Na_2SO_4, filtered and concentrated in vacuum. The crude was purified by flash-chromatography to yield the desired thio-alkylated or arylated β-lactam.

1-(benzylthio)-4-oxoazetidin-2-yl acetate (1c)

Following GP1, dibenzyldisulfide (246 mg, 1 mmol) was reacted with starting material **1** (129 mg, 1 mmol) yielding compound **1c** as a yellow oil (100 mg, 40%) after purification by flash-chromatography (cyclohexane/EtOAc 75:25). IR (film, cm^{-1}) 3085, 3061, 2960, 2923, 1779, 1751, 1429, 1225; ^{1}H NMR (400 MHz, $CDCl_3$) δ (ppm) 7.40 – 7.27 (m, 5H), 5.62 – 5.57 (m, 1H), 4.13 (d, J = 12.7 Hz, 1H), 3.93 (d, J = 12.7 Hz, 1H), 3.23 (dd, J = 15.3, 4.1, Hz, 1H), 2.92 (d, J = 15.3 Hz, 1H), 2.04 (s, 3H); ^{13}C NMR (100 MHz, $CDCl_3$) δ (ppm) 169.8, 167.8, 135.2, 129.3, 128.6, 127.7, 78.9, 46.1, 42.9, 20.7; ESI-MS (Rt = 7.7 min) m/z 252 $[M+H]^+$, 269 $[M+H_2O]^+$. Exact mass: calculated for $C_{12}H_{13}NO_3S$ as 251.0616, observed 274.0509 $[M+Na]^+$.

1-(isopropylthio)-4-oxoazetidin-2-yl acetate (1d)

Following GP1, diisopropyldisulfide (125 μL, 1 mmol) was reacted with starting material **1** (129 mg, 1 mmol) yielding compound **1d** as a yellow oil (57 mg, 28%) after purification by flash-chromatography (cyclohexane/EtOAc 75:25). IR (film, cm^{-1}) 2965, 2927, 1783, 1753, 1373, 1227; ^{1}H NMR (400 MHz, $CDCl_3$) δ (ppm) 6.06 (dd, J = 4.2, 1.6 Hz, 1H), 3.39 (dd, J = 15.4, 4.2 Hz, 1H), 3.23 (sept, J = 6.7 Hz, 1H), 3.01 (dd, J = 15.4, 1.6 Hz, 1H), 2.12 (s, 3H), 1.26 (d, J = 6.7 Hz, 3H), 1.23 (d, J = 6.7 Hz, 3H); ^{13}C NMR (100 MHz, $CDCl_3$) δ (ppm) 170.0, 168.8, 79.4, 46.1, 41.6, 21.5, 21.1, 20.8; ESI-MS (R_t = 6.0 min) m/z 204 $[M+H]^+$, 226 $[M+Na]^+$. Exact mass: calculated for $C_8H_{13}NO_3S$, 203.0616, observed 226.0509 $[M+Na]^+$.

4-oxo-1-(propylthio)azetidin-2-yl acetate (1e)

Following GP1, propyldisulfide (141 μL, 1 mmol) was reacted with starting material **1** (129 mg, 1 mmol) yielding compound **1e** as a yellow oil (134 mg, 66%) after purification by flash-chromatography (cyclohexane/EtOAc 75:25). IR (film, cm^{-1}) 2965, 2934, 1785, 1755, 1375, 1290; ^{1}H NMR (400 MHz, $CDCl_3$) δ (ppm) 6.04 (dd, J = 4.1, 1.5 Hz, 1H), 3.36 (dd, J = 15.3, 4.1 Hz, 1H), 2.99 (dd, J = 15.3, 1.5 Hz, 1H), 2.78 – 2.64 (m, 2H), 2.11 (s, 3H), 1.70 – 1.59 (m, 2H), 0.99 (t, J = 7.4 Hz, 3H); ^{13}C NMR (100 MHz, $CDCl_3$) δ (ppm) 170.0, 168.4, 79.1, 46.2, 41.0, 21.9, 20.8, 12.9; ESI-MS (R_t = 6.3 min) m/z 204 $[M+H]^+$, 226 $[M+Na]^+$. Exact mass calculated for $C_8H_{13}NO_3S$ 203.0616, observed = 226.0510 $[M+Na]^+$.

1-(benzo[d]thiazol-2-ylthio)-4-oxoazetidin-2-yl acetate (1f)

Following GP1, 2,2'-dithiobis(benzothiazole) (333 mg, 1 mmol) was reacted with 4-acetoxy-azetidin-2-one **1** (129 mg, 1 mmol) yielding compound **1f** as a yellow oil (243 mg, 83%) after purification by flash-chromatography (cyclohexane/EtOAc 75:25). IR (film, cm^{-1}) 2925, 2853, 1798, 1755, 1467, 1428, 1279; ^{1}H NMR (400 MHz, $CDCl_3$) δ (ppm) 7.87 (d, J = 8.1 Hz, 1H), 7.78 (d, J = 8.1 Hz, 1H), 7.43 (dd, J = 8.1, 1.2 Hz, 1H), 7.32 (dd, J = 1.2, 8.1Hz, 1H), 6.39 (dd, J = 4.4, 1.8 Hz, 1H), 3.64 (dd, J = 15.6, 4.4 Hz, 1H), 3.26 (dd, J = 15.6, 1.8 Hz, 1H), 2.10 (s, 3H); ^{13}C NMR (100 MHz, $CDCl_3$) δ (ppm) 20.6, 46.8, 79.0, 121.1, 122.4, 124.9, 126.4, 135.2, 153.5, 166.8, 166.9, 169.8; ESI-MS (R_t = 8.2 min) m/z = 295 $[M+H]^+$. Exact mass calculated for $C_{12}H_{10}N_2O_3S_2$ 294.0133, observed = 317.0026 $[M+Na]^+$.

1-((4-methoxyphenyl)thio)-4-oxoazetidin-2-yl acetate (1g)

Following GP1, *p*-methoxyphenyldisulfide (278 mg, 1 mmol) was reacted with 4-acetoxy-azetidin-2-one **1** (129 mg, 1 mmol) yielding compound **1g** as a yellow oil (174 mg, 65%) after purification by flash-chromatography (cyclohexane/EtOAc 75:25). IR (film, cm^{-1}) 3065, 3008, 2963, 2942, 1780, 1754, 1591, 1493, 1288; ^{1}H NMR (400 MHz, $CDCl_3$) δ (ppm) 7.58 – 7.53 (m, 2H), 6.89 – 6.84 (m, 2H), 6.11 (dd, J = 4.2, 1.6 Hz, 1H), 3.80 (s, 3H), 3.30 (dd, J = 15.2, 4.2 Hz, 1H), 3.00 (dd, J = 15.2, 1.6 Hz, 1H), 2.03 (s, 3H); ^{13}C NMR (100 MHz, $CDCl_3$) δ (ppm) 170.1, 167.4, 160.9, 134.8, 126.2, 114.7, 78.1, 55.4, 45.9, 20.7; ESI-MS (R_t = 7.8 min) m/z 268 $[M+H]^+$. Exact mass calculated for $C_{12}H_{13}NO_4S$ 267.0565, observed = 290.0460 $[M+Na]^+$.

(2R,3R)-1-(benzylthio)-3-((R)-1-((tert-butyldimethylsilyl)oxy) ethyl)-4-oxoazetidin-2-yl acetate (2c)

Following GP1, dibenzyldisulfide (246 mg, 1 mmol) was reacted with (2*R*,3*R*)-3-((*R*)-1-((*tert*-butyldimethylsilyl)oxy)ethyl)-4-oxoazetidin-2-yl acetate **2**, (287 mg, 1 mmol) yielding compound **2c** as a yellow oil (74 mg, 18%) after purification by flash-chromatography (cyclohexane/EtOAc 80:20). IR (film, cm^{-1}) 2955, 2929, 2886, 2856, 1790, 1754, 1471, 1375, 1222; $[\alpha]_D^{20}$ = – 10 (c = 1.0, CH_2Cl_2); ^{1}H NMR (400 MHz, $CDCl_3$) δ (ppm) 7.35 – 7.29 (m, 5H), 6.09 (d, J = 1.4 Hz, 1H), 4.15 – 4.10 (m, 1H), 4.04 (q, J_{AB} = 12.4 Hz, 2H), 3.14 (dd, J = 3.8, 1.4 Hz, 1H), 2.03 (s, 3H), 1.22 (d, J = 6.3 Hz, 3H), 0.84 (s, 9H), 0.05 (s, 3H), 0.02(s,3H); ^{13}C NMR (100 MHz, $CDCl_3$) δ (ppm) 169.8, 169.2, 134.9, 129.4, 128.6, 127.7, 81.1, 66.3, 64.3, 43.5, 25.6, 22.1, 20.8, 17.8, -4.4, -5.1; ESI-MS (R_t = 14.4 min) m/z 432 $[M+Na]^+$.

(2R,3R)-3-((R)-1-((tert-butyldimethylsilyl)oxy)ethyl)-1-(isopropylthio)-4-oxoazetidin-2-yl acetate (2d)

Following GP1, isopropyldisulfide (125 μL, 1 mmol) was reacted with starting material **2** (287 mg, 1 mmol) yielding compound **2d** as a yellow oil (96 mg, 27%) after purification by flash-chromatography (cyclohexane/EtOAc 40:60). IR (film, cm^{-1}) 2958, 2929, 2857, 1791, 1754, 1461, 1375, 1222; $[\alpha]_D^{20}$ = – 18 (c = 1.0, CH_2Cl_2); ^{1}H NMR (400 MHz, $CDCl_3$) δ (ppm) 6.21 (d, J = 1.4 Hz, 1H), 4.22 (qd, J = 6.3, 3.2 Hz, 2H), 3.23 (sept, J = 6.7 Hz, 1H), 3.19 (dd, J = 3.2, 1.4 Hz, 1H), 2.13 (s, 3H), 1.28 (d, J = 6.7 Hz, 3H), 1.24 (d, J = 6.3, 3H), 1.23

(d, J = 6.7 Hz, 3H), 0.85 (s, 9H), 0.06 (s, 3H), 0.04 (s, 3H); ^{13}C NMR (100 MHz, $CDCl_3$) δ (ppm) 170.2, 169.8, 81.3, 66.4, 64.1, 41.6, 29.7, 25.7, 22.2, 21.8, 21.01, 20.99, 17.9, -4.5, -5.0; ESI-MS (R_t = 13.6 min) m/z 384 $[M+Na]^+$.

(2R,3R)-3-((R)-1-((tert-butyldimethylsilyl)oxy)ethyl)-4-oxo-1-(propylthio)azetidin-2-yl acetate (2e)

Following GP1, propyldisulfide (141 μL, 1 mmol) was reacted with starting material **2** (287 mg, 1 mmol) yielding compound **2e** as a yellow oil (133 mg, 37%) after purification by flash-chromatography (cyclohexane/EtOAc 90:10). IR (film, cm^{-1}) 2958, 2931, 2884, 2857, 1790, 1753, 1462, 1362, 1224; $[\alpha]_D^{20}$ = – 14 (c = 1, CH_2Cl_2); ^{1}H NMR (400 MHz, $CDCl_3$) δ (ppm) 6.17 (d, J = 1.2 Hz, 1H), 4.19 (qd, J = 6.3, 3.2 Hz, 1H), 3.17 – 3.13 (m, 1H), 2.77 – 2.62 (m, 2H), 2.11 (s, 3H), 1.71 – 1.58 (m, 2H), 1.21 (d, J = 6.3 Hz, 3H), 0.98 (t, J = 7.3 Hz, 3H), 0.83 (s, 9H), 0.04 (s, 3H), 0.01 (s, 3H); ^{13}C NMR (100 MHz, $CDCl_3$) δ (ppm): 169.7, 80.9, 66.3, 64.0, 41.1, 25.6, 22.2, 22.0, 20.9, 17.8, 12.9, -4.6, -5.1; ESI-MS (R_t =13.7 min) m/z = 384 $[M+Na]^+$.

Protein production and purification

The recombinant production and the purification of the Ldt_{Mt2} (UniProt code O53223; Rv2518c) construct comprising the B (immunoglobulin-like) and C (catalytic, transpeptidase) domains (the BC module) including residues 149 – 408 has been carried out as described previously (Böth et al., 2013). The protein preparations were concentrated to 28.8 mg/mL in the buffer 25 mM Tris-HCl, 150 mM NaCl, pH 8.0, flash-frozen in liquid nitrogen in 55 μl aliquots and stored at -80°C until further use.

Adduct formation at the active site cysteine

The sole sulfhydryl group at the active site Cysteine-354 is detected using 5,5'-dithio-bis-(2-nitrobenzoic acid) (DTNB, Sigma-Aldrich) that derivatizes the free thiol group and releases a stoichiometric amount of thio-nitrobenzoate that can be monitored by absorbance at 412 nm. The stock solution of 100 mM DTNB is prepared in 95% ethanol, kept at -20°C and diluted freshly in the reaction buffer (0.1M potassium phosphate pH 8.0 and 1 mM EDTA) to 10 mM working solution prior to the measurements. The sample of the Ldt_{Mt2} BC-module at 50 μM concentration and the tested compounds at 1.0 mM concentration were incubated in 50 μl total volume for 7 minutes and mixed with 12 μl of DTNB working solution in CORNING 96-well half area assay plates (No. 3994, Sigma-Aldrich). The absorption is monitored at 412 nm using a Bio-tek Synergy HT plate reader. A cysteine standard curve was generated using 250, 125, 62.5, 31.3, 15.6, 7.8, 3.9 μM L-cysteine while protein standard curve is generated using protein samples at 300, 150, 75, 37.5, 18.8, 9.4, 4.7, 2.35 μM concentration, validating the assay and ensuring the reactivity of the single cysteine sidechain. Reactions were carried out in triplicates, mean A_{412} values and standard deviation are plotted.

The kinetics of the adduct formation was investigated using the DTNB-based assay as above. The Ldt_{Mt2} BC-module at 50 μM concentration and the tested compounds at 50μM concentration were mixed a 50 μl total volume, and mixed with 12 μl of DTNB reagent at various time-points. The time ranges were 0-4500 seconds for **1a**, 0-550 seconds for **1b** and **1c**, and 0-1100 seconds for **1e** and **1g**. The absorbance at 412 nm was monitored in CORNING 96-well half area assay plates (No. 3994, Sigma-Aldrich) using a Biotek Synergy HT plate reader. The absorbance values were evaluated using single turnover kinetic model fitting an exponential curve to derive the rate constant (k_{obs}) of the reaction as previously (Steiner et al., 2017). All reactions were carried out as triplicates.

Adduct stability was monitored in the presence of the potential acceptor substrate *meso*-Dap. The pre-formed protein-adducts were prepared by mixing the protein at 58 μM protein to 58 μM of the tested *N*-thio-β-lactam compounds (**1a**, **1b**, **1c**, **1e**, **1g**) or meropenem and confirming the successful block on the active site Cys354 by testing a sample in the DTNB-assay and recording the absorbance at 412 nm. Subsequently *meso*-Dap (Sigma-Aldrich) were added at 4 mM concentration to these reactions resulting in protein-adduct concentrations at 50 μM. 50 μl samples were withdrawn at various time points (0-12 minutes), developed in the DTNB-assay by mixing these to 12 μl DTNB-reagent and the A_{412} values were recorded. The reactions were performed in triplicates, mean A412 values and standard deviation are plotted.

Mass spectrometric analysis of covalent adduct formation

The reagents used to prepare mass spectrometry samples were acetonitrile (VWR), formic acid (Merck) and TCEP (Tris(2-carboxyethyl)phosphine, Sigma-Aldrich). Samples of Ldt_{Mt2}, 30 μg amounts were dispensed in 20 μL water (corresponding to a concentration of 52 μM) with the β-lactam compounds tested at 1 mM concentrations (similar results obtained with 60 μM compound to 2 mM and 4 mM compound used) and incubated for 30 min at 22 °C. Subsequently, the samples were diluted in 0.5 mL denaturing buffer (5%(v/v) acetonitrile, 0.1%(v/v) formic acid, 0.5 mM TCEP). Mass spectra were acquired on a Micromass LCT ToF modified for analysis of intact protein complexes (MS Vision, The Netherlands) equipped with an offline nanospray source. Samples were injected directly using gold-plated borosilicate capillaries (ThermoScientific). The capillary voltage was 1.5 kV and the RF lens 1.5 kV. The cone voltage was 100 V and the pressure in the ion source was maintained at 4.0 mbar. Spectra were combined and deconvoluted with the Maximum Entropy 1 algorithm from the MassLynx 4.1 software suite (Waters Corp.) to obtain the molecular weights of the protein molecules and the protein–antibiotic adducts.

Adduct stability was monitored in time resolved studies by exposing the protein at 40 μM and the compounds at 50 μM in a total volume of 30 μl and retrieving 2-2 μl samples at various time points (0 sec, 60sec, 1800 sec and 360 minutes). The 2 μl samples were mixed with 48 μl denaturing buffer (5% (v/v) acetonitrile, 0.1% (v/v) formic acid, 0.5 mM TCEP) and analyzed as above.

Protein crystallization and structure determination

Crystals of the Ldt_{Mt2} BC-module were produced by the vapor diffusion method in hanging drop format at 20 °C using the crystallization buffer consisting of 0.1 M Na-citrate, 17.5% PEG 6000. The protein-adduct formed with **1g** and **1b** was produced by adding

the compounds at 4 mM concentration to the protein solution (1.0 mM) and incubating this mixture at 20 ºC for 1 to 10 minutes. The preformed protein-adducts (1 μl volumes) were than mixed with the crystallization buffer (1 μl volumes) and incubated over 1.0 mL of the crystallization buffer. The crystals were cryo-protected by dipping them in 0.1 M Na-Citrate pH 4.25, 25% PEG 6000. The protein-adducts with **1a**, **1c**, and **1e**, and were formed by soaking native crystals of the Ldt_{Mt2} BC-module in a drop containing 0.1 M Bis-Tris pH 6.2, 150 mM NaCl, 0.3 M Na-acetate pH 5.2, 25% PEG 6000, and the compound at 4.0 mM concentration for 60-120 minutes. Several crystals were evaluated, typically the adduct formation was completed within 60 minutes soaking time, however the datasets with the best adduct occupancy and resolution were used to determine the structure.

X-ray diffraction data sets were collected at the Biomax beamline of the MAX-IV synchrotron (Lund, Sweden, EU). The diffraction datasets were indexed and integrated using XDS (Kabsch, 2010) scaled by AIMLESS from the CCP4i suite (Winn et al., 2011). The structures were solved by molecular replacement using MOLREP (Vagin and Teplyakov, 2010) and the ligand free structure derived from the structure of the same module (PDB: 5LBG) (Steiner et al., 2017) as search model. The adduct restrains were prepared by PRODRG (Schüttelkopf and van Aalten, 2004) and the models were completed by manual model building in COOT (Emsley et al., 2010) interspersed with refinement by REFMAC-5 (Murshudov et al., 2011) runs. The crystallographic models were validated using COOT and MOLPROBITY (Williams et al., 2018). Macromolecular interfaces and solvent accessible surface areas were calculated by PISA (Krissinel and Henrick, 2007) and AREAIMOL, B-factors are analyzed by BAVERAGE (Winn et al., 2011). The structure figures were prepared using PyMOL (http://www.pymol.org) and LigPlot+ (Laskowski and Swindells, 2011). The refined models and the structure factors are deposited with the Protein Data Bank (wwPDB Acc. Nr.: 7A1C, 7A0Z, 7A1E, 7A11, 7A10).

Determination of antimycobacterial activity

Mycobacterium tuberculosis strain identification, isolation, and drugs susceptibility test (DST) were performed at S. Orsola-Malpighi University Hospital, Microbiology Unit, Bologna, Italy. The reference strain H37Rv (ATCC 25618) and four clinical isolates, selected on the basis of DST results to first-line drugs obtained by the ''gold standard'' automatic Bactec MGIT 960 (MGIT, Becton Dickinson), were used in this study. The critical concentrations (CC) tested by MGIT in the selected isolates were: 0.1 and 0.4 μg/mL for isoniazid (INH), 1.0 μg/mL for rifampicin (RIF); 5.0 and 7.5 μg/mL for ethambutol (EMB), and 100 μg/mL for pyrazinamide (PZA), according to the Clinical and Laboratory Standard Institute procedures (Wayne, 2018). Drug-susceptible isolates were sensitive to first-line drugs, while MDR-1 and MDR-2 were Multi Drugs Resistant (MDR) strains because of resistance to INH and RIF. In addition, the critical concentrations of β-lactam compounds in the range of 5, 10, 20, 30, 40, 50 and 100 μg/mL of were tested by MGIT on the drug-susceptible strain. The results are shown in the supplemental information in Table S3.

The minimal inhibitory concentration (MIC) values were determined using a broth microdilution method performed in 96-well U bottom plates by Sensititre Mycobacterium tuberculosis MYCOTBI Plate (Thermo Scientific™ USA) for the reference strain H37Rv, the drug susceptible, and the MDR-1 and MDR-2 isolates (Hall et al., 2012). MIC values were read using the mirrored Sensititre Manual Viewbox (Thermo Scientific™ USA) after approximately 4 weeks of incubation when the growth was detected in the drug-free control (GC) wells. The results are shown in the supplemental information in Table S4. Molecular tests in the used MDR isolates were performed to detect mutations in the rpoB, katG or inhA (GenoType MTBDRplus 2.0, Bruker, Germany) and gyrA, gyrB, rrs and eis genes (MTBDRsl 2.0, Bruker, Germany) in order to confirm phenotypic results.

The tested β-lactam compounds were dissolved in 1 mL of DMSO, then diluted with sterile water to obtain 0.5 mg/mL stock solutions. Five 2-fold serial dilutions were prepared starting from stock solutions resulting the final concentrations of 2.5, 5, 10, 20, and 40 μg/mL. Clavulanic acid was added at a final concentration of 5 μg/mL (Li et al., 2018; Diacon et al., 2016). Colonies (3 to 5) of the tested strains were picked from LJ slants and adjusted in a Saline Tween with Glass Beads solution (Thermo Scientific™USA) to 1.5 x 10^8 CFU/mL (0.5 Mc Farland). The suspension was diluted 100-fold in Middlebrook 7H9 with OADC Broth (Thermo Scientific™) and 100 μL of *M. tuberculosis* suspension was inoculated in each well. The effect of DMSO was evaluated adding the highest DMSO concentration (4%) used to dissolve the molecules into GC wells. The β-lactam compounds were tested in triplicate against each isolate, with and without 5 μg/mL clavulanic acid (Merck KGaA, Germany). Meropenem was tested (0.125-64 μg/mL), with and without 5μg/mL of clavulanic acid, as control compounds in the same setup. The plates were sealed and incubated at 37°C for approximately 3 weeks in a non-CO_2 incubator. MIC values, defined as the lowest concentration of the tested compound able to inhibit detectable growth of the microorganism, were expressed in μg/mL.

QUANTIFICATION AND STATISTICAL ANALYSIS

The spectrophotometric absorbance data for enzyme kinetics was recorded in triplicate measurement, mean values and standard deviation indicated by the error bars was plotted on Figure 2 panels B, C and E. The time dependent change in absorbance were plotted against time and the kinetic constants k_{obs} of covalent adduct formation were derived from the exponential fits using the single turnover kinetic model $A = A_0 + A_1 e^{-kt}$ in the OriginLab software (OriginLab, Northampton, Massachusetts, USA). The kinetic constant is reported with the standard error derived from the fit.

The quantitative data obtained from the mycobacterial cultures were reported as Minimum Inhibitory Concentrations (MIC) values expressed in μg/mL.